DAHLGREN DIVISION
NAVAL SURFACE WARFARE CENTER
Dahlgren, Virginia 22448-5100

(1)

NSWCDD/TR-96/10

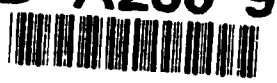

BENCHMARK PROBLEM FOR RADAR RESOURCE ALLOCATION AND TRACKING MANEUVERING TARGETS IN THE PRESENCE OF ECM

BY W. D. BLAIR G. A. WATSON
SYSTEMS RESEARCH AND TECHNOLOGY DEPARTMENT

SEPTEMBER 1996

REPORT DOCUMENTATION PAGE

Form Approved
OBM No. 0704-0188

1. AGENCY USE ONLY (Leave blank)	2. REPORT DATE	3. REPORT TYPE AND DATES COVERED
	September 1996	

4. TITLE AND SUBTITLE
BENCHMARK PROBLEM FOR RADAR RESOURCE ALLOCATION AND TRACKING MANEUVERING TARGETS IN THE PRESENCE OF ECM

5. FUNDING NUMBERS

6. AUTHOR(s)
W. D. Blair G. A. Watson

7. PERFORMING ORGANIZATION NAME(S) AND ADDRESS(ES)
Commander
Naval Surface Warfare Center, Dahlgren Division (Code B32)
17320 Dahlgren Road
Dahlgren, VA 22448-5100

8. PERFORMING ORGANIZATION REPORT NUMBER
NSWCDD/TR-96/10

9. SPONSORING/MONITORING AGENCY NAME(S) AND ADDRESS(ES)

10. SPONSORING/MONITORING AGENCY REPORT NUMBER

11. SUPPLEMENTARY NOTES

12a. DISTRIBUTION/AVAILABILITY STATEMENT
Approved for public release; distribution is unlimited.

12b. DISTRIBUTION CODE

13. ABSTRACT (Maximum 200 words)

This report presents a benchmark problem for tracking maneuvering targets. The benchmark problem involves beam pointing control of a phased-array (i.e., agile beam) radar against highly maneuvering targets in the presence of False Alarms (FAs) and Electronic Counter Measurements (ECM). The testbed simulation described in this report includes the effects of target amplitude fluctuations, beamshape, missed detections, FAs, finite sensor resolution, target maneuvers, and track loss. Multiple waveforms are included in the benchmark so that the radar energy can be coordinated with the tracking algorithm. The ECM includes a Standoff Jammer (SOJ) broadcasting wideband noise and targets attempting Range Gate Pull Off (RGPO). The limits on the position and maneuverability of the targets are given along with descriptions of six target trajectories. The "best" tracking algorithm is the one that minimizes a weighted average of the radar energy and radar time, while satisfying a constraint of 4 percent on the maximum number of lost tracks. The report presents the radar model, the ECM techniques, the target scenarios, and performance criteria for the benchmark. A MATLAB computer program, which will simulate the adaptive tracking of maneuvering targets as a benchmark problem, is included on a computer diskette so that other researchers can implement and evaluate their algorithm with minimal effort.

14. SUBJECT TERMS	15. NUMBER OF PAGES
phased-array radar, Electronic Counter Measurements, ECM, False Alarm, FA, tracking algorithm, Standoff Jammer, SOJ, Range Gate Pull Off, RGPO	68
	16. PRICE CODE

17. SECURITY CLASSIFICATION OF REPORT	18. SECURITY CLASSIFICATION OF THIS PAGE	19. SECURITY CLASSIFICATION OF ABSTRACT	20. LIMITATION OF ABSTRACT
UNCLASSIFIED	UNCLASSIFIED	UNCLASSIFIED	SAR

FOREWORD

As naval operations move into littoral environments and address Tactical Ballistic Missiles Defense (TBMD), the demand for shipboard sensor resources will increase significantly. Furthermore, threat trends indicate that the conditions under which hostile targets can be engaged successfully are becoming more difficult to achieve. In contrast to addressing these challenging problems by focusing on the procurement of more information through more efficient hardware and signal processing or additional sensors, this report focuses on the efficient utilization of the sensor information through modern tracking algorithms with adaptive revisit times of a phased array radar. This adaptive tracking technology is presented in the form of a benchmark problem.

While the problem of tracking maneuvering targets has been studied extensively, the authors were the first to define in the literature standard problems that could be used for comparison and evaluation of tracking algorithms. The lack of benchmark problems has hindered the progress of the target tracking community with respect to individual applications of research to many "real world" problems. Thus, many researche. · and their solutions have not been considered during the development and demonstration of systems with advanced technology. In order to address this lack of benchmark problems, the authors organized invited sessions at the 1994 and 1995 American Control Conferences and invited researchers to present solutions to benchmark problems. The benchmark problems included many real world issues such as finite sensor resolution, track initiation, beam pointing control, false alarms, and Electronic Counter Measures (ECM). The benchmark problem presented in this report was developed from the lessons learned at the American Control Conferences. A computer program that will simulate the adaptive tracking of maneuvering targets as a benchmark problem is included on a diskette so that other researchers can implement and evaluate their algorithm with minimal effort. This benchmark has been accomplished through funding from the NSWCDD In-house Laboratory Independent Research (ILIR) Program sponsored by the Office of Naval Research.

This report has been reviewed by Dr. T. R. Rice, Technical Lead, Target Tracking and Signal Processing; and R. N. Cain, Head, Combat Systems Technology Group.

Approved by:

MARY E. LACEY, Head
Systems Research and Technology Department

CONTENTS

ILLUSTRATIONS

TABLES

CHAPTER 1
INTRODUCTION

While the problem of tracking maneuvering targets has been studied extensively [1-5], no standard or benchmark problems had been identified in the literature for comparison and evaluation of proposed algorithms until [6,7]. While design objectives, operating conditions, and system constraints differ significantly between tracking problems, clearly defined benchmark problems in the areas of target tracking such as data association, multiple target tracking, and tracking maneuvering targets have been found to be very helpful in the assessment and comparison of existing algorithms. The lack of benchmark problems has hindered the progress of the target tracking community with respect to many "real-world" problems, and thus, many researchers and their solutions have been omitted from consideration during the development and demonstration of systems with advanced technology.

The first benchmark [6] included many of the features of an actual phased array radar and realistic scenarios as well as many of the restrictions that occur in a "real-world" environment. The testbed simulation for the first benchmark problem included the effects of target amplitude fluctuations, beamshape, missed detections, finite sensor resolution, target maneuvers, and track loss. The tracking requirements were specified in terms of limits on the position and maneuverability of the targets rather than by a set of scenarios. The "best" tracking algorithm was determined to be the one that minimized the average number of radar dwells while satisfying a constraint of 4 percent on the maximum number of lost tracks. Using a filter performance criterion based on system performance helped to focus the efforts of the researchers onto those issues that are important to the system designers and, thus, illustrated the benefits of modern tracking (*i.e.*, data processing) through the benchmark. However, the benchmark of [6] did not include False Alarms (FAs) (*i.e.*, false detections) or Electronic Counter Measures (ECM), which are two critical elements of any "real-world" tracking problem [8,9]. While parameter control and tracking in the presence of false alarms was considered for a phased array radar in [10], no standard problem was available to the authors to assess the performance of their new techniques relative to other existing techniques.

This report extends the benchmark of [6] to include the effects of FAs and ECM.[1] The inclusion of FAs is accompanied with multiple radar waveforms so that the waveform energy

[1] While this report has the same objective as [7], this report and the corresponding simulation program include many improvements over that of [7].

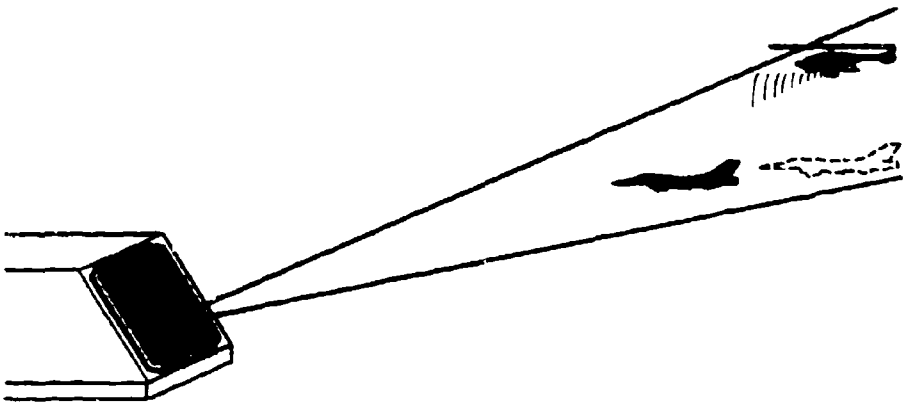

Figure 1.1 Illustration of Beam Pointing Control of a Phased Array Radar

can be coordinated with the tracking algorithm. The ECM includes Range Gate Pull Off (RGPO) on the target and a Standoff Jammer (SOJ) broadcasting wideband noise. Figure 1.1 gives an illustration of the problem, where the helicopter is a SOJ and the dotted aircraft illustrates the effects of a RGPO. If the pointing of the radar beam, denoted by the straight solid lines, is bad, the target will not be detected. For this benchmark the "best" tracking algorithm is the one that minimizes a weighted average of the radar energy and radar time, while satisfying a constraint of 4% on the maximum number of lost tracks.

Figure 1.2 shows a block diagram of the MATLAB[2] simulation program for the benchmark, while additional documentation on the use of the simulation program is given in Appendix B. Each benchmark participant codes his tracking algorithm in the block entitled "Tracking Algorithm," which is given the range, bearing, and elevation of the initial detection of the target. For each experiment, the tracking errors, radar energy, and radar time are saved. After the last experiment of the Monte Carlo simulation, the average tracking errors, average radar energy per second, and average radar time per second[3] are computed for maintained tracks and the percent of lost tracks is also computed. A constraint of 4% is to be imposed on the number of lost tracks. A track is considered lost if the distance between the true target position and the target position estimate exceeds one beamwidth in angle or 1.5 range gates. When FAs and ECM are present in an actual radar system, algorithms for reacquiring the target and "coasting" the target tracks through jamming signals are required in order to maintain a track. However, in this benchmark problem, the SOJ power is limited so that the it can be defeated with one of the higher energy waveforms.[4]

[2] MATLAB is a trademark of The MathWorks, Inc., Natick, MA.

[3] This is inversely proportional to the average sample period. More details on this are given in Chapter 6.

[4] This restriction is made to limit the scope of the problem and reduce the problems associated with declaring a track as lost.

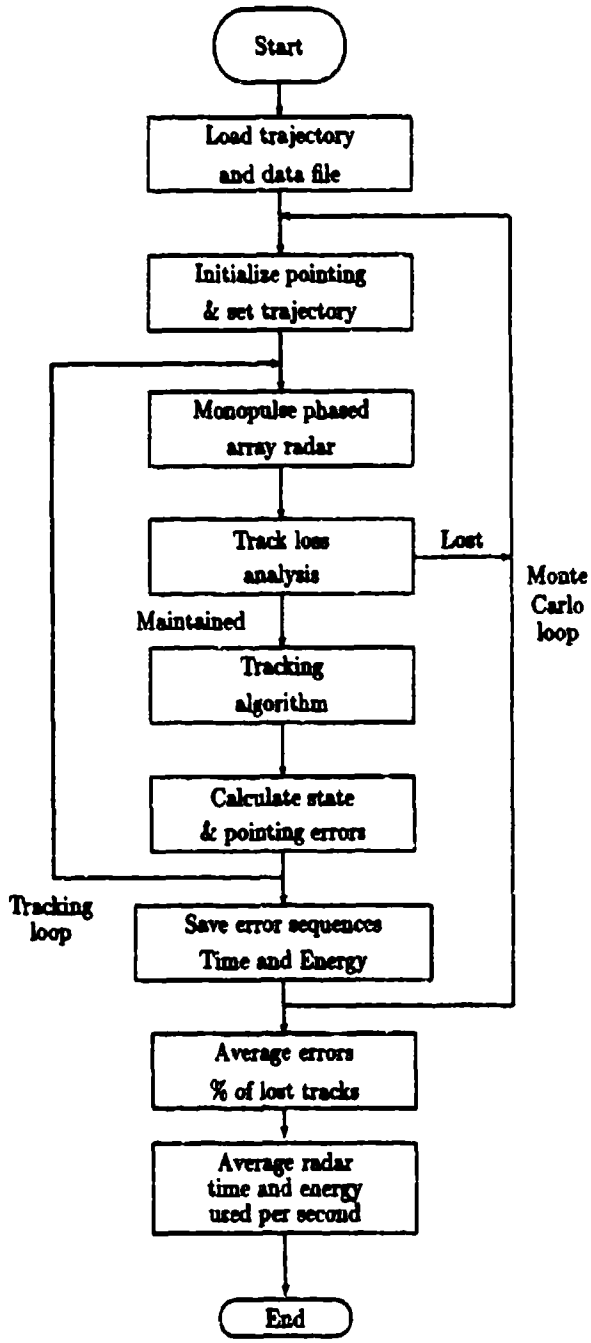

Figure 1.2 Block Diagram of Simulation Program

Since track initiation is very expensive with respect to radar time and energy, the emphasis of this benchmark is on maintaining tracks with an allowance for track reacquisition within a few radar dwells.[5]

The radar model simulation includes the effects of target amplitude fluctuations, beamshape, missed detections, finite resolution, FAs, an SOJ, and RGPO. The radar performs search dwells, monopulse track dwells, and monopulse passive dwells. Eight radar waveforms that differ primarily in the pulse length are available for control (*i.e.*, selection) from the tracking (and radar management) algorithm. Since a waveform with a longer pulse length provides a higher Signal-to-Noise Ratio (SNR) at the cost of more radar energy, the proper coordination of the waveform selection with the tracking algorithm is an important "real-world" issue to be addressed by each participant. For example, a higher target SNR results in fewer FAs at a cost of more radar energy. RGPO and standoff jamming in the mainlobe and sidelobes are included in the benchmark problem. In RGPO, the target under track repeats with delay the radar pulse to pull the radar range gate off the target so that no detection of the true target will occur. The time delay is controlled so that the false target is separated from the target with linear or quadratic motion. For tracking an SOJ, passive measurements of the jammer position (*i.e.*, angle only) are provided by the radar at the request of the tracking algorithm, with bearing and elevation angles for pointing. Thus, the tracking algorithm will be required to track one target and one jammer. When the jammer is in the mainlobe of the radar beam pattern, the target return will be corrupted or hidden by the jammer signal. When the jammer is in one of the sidelobes, the SNR for the target will be reduced. The initial bearing and elevation of the jammer will be given to the tracking algorithm.

The targets exhibit Radar Cross Section (RCS) fluctuations according to the Swerling 3 type and perform as much as 7 g of lateral acceleration and 2 g of longitudinal acceleration. Target range can vary from 20 to 100 km, while the target elevation angle can vary from 2° to 30°. Since only one face of the phased array radar is used, the bearing (or azimuth) of the target will be confined to ±60°. The average RCSs of the targets are large enough so that an average SNR of 18 dB is achievable with the highest energy waveform. The SOJ remains at ranges near 150 km and performs less than 2 g of acceleration.

Results of Previous Benchmark Efforts

An invited session was organized at the 1994 American Control Conference (ACC) with the first benchmark as the theme for the session. The benchmark problem was presented, along with four different approaches to the problem. The results of the invited session [11-13] and other studies such as [14] provided relative comparisons of different tracking algorithms on the first benchmark. The $\alpha - \beta$ filter provided an average sample period of 0.85 s, while

[5] Reacquisition is allowed if it can be accomplished before the estimation errors exceed the criteria for a track being considered lost.

a standard Kalman filter with a nearly constant velocity motion model provided an average sample period of about 1 s. Thus, for an order of magnitude increase in computations, the Kalman filter provided only an 20% increase in the average sample period. A two-model Interacting Multiple Model (IMM) algorithm provided an average sample period of 1.3 s, while a three-model IMM algorithm provided an average sample period of 1.5 s. Incorporating adaptive revisit times with a three-model IMM algorithm provided an average sample period of 2.3 s, for about 1.6 orders of magnitude increase in computations relative to the $\alpha - \beta$ filter. An H-Infinity filter solution was originally included in the invited session at the 1994 ACC, but the authors withdrew the paper when they concluded that the H-Infinity filter provided no significant advantage over the Kalman filter. [15].

The panel discussion held during the invited session at the 1994 ACC revealed the importance of tracking maneuvering targets in the presence of ECM. Thus, a second invited session was organized for the 1995 ACC with a new benchmark [7] that included false alarms and ECM. However, the difficulty of the new benchmark, discrepancies in the calculation of the radar energy, and deficiencies in the simulation program resulted in no quantitative results for comparison of the performances of the different algorithms. Qualitatively, the IMM algorithm and Multiple Hypotheses Tracking (MHT) yielded comparable results, with the MHT algorithm being 1 to 2 orders of magnitude costlier in computations.

Many of the deficiencies associated with the benchmark problem at the 1995 ACC were corrected to produce the benchmark problem described in this report. Reference [16] presents an IMMPDAF solution to this benchmark problem, while [17] presents an adaptive Kalman filter solution. The adaptive Kalman filter provided an average sample period near 1 s, while the IMMPDAF provided an average sample period near 2 s. The adaptive Kalman filter also required about 30% more energy than the IMMPDAF. To date, no results for MHT are available to assess its performance relative to these two solutions.

Organization of the Report

This report is organized as follows. Chapter 2 describes the radar model, while Chapter 3 discusses the SOJ and RGPO. The target trajectories are presented in Chapter 4, along with the average RCS for each target and the timing for the use of the RGPO. Chapter 5 discusses the inputs and outputs of the tracking algorithm. The criteria for evaluating the performance of the tracking algorithm are given in Chapter 6, and concluding remarks are given in Chapter 7.

CHAPTER 2
RADAR MODEL

The radar is a 4 GHz phased array using amplitude-comparison monopulse with uniform illumination across the array. Each radar dwell consists of one phase/frequency discrete-coded pulse [18]. The range gate is approximately 1575 meters for a track dwell and 10 km for a search dwell, with the number of range bins varying from 70 to 444 depending upon the waveform and dwell type. The radar beam is quasi-circular with the beamwidth increasing as the beam is steered off the broadside direction. The radar beam has a 3 dB beamwidth of $\theta_{BW} = 2.4°$ on broadside (*i.e.*, normal to the face of the array) and $\theta_{BW} = 4.5°$ at a broadside angle of 60°. The two-way radar beam has a 3 dB beamwidth of $\theta_{BW} = 1.6°$ on broadside and $\theta_{BW} = 3.2°$ at a broadside angle of 60°. The beam is pointed to the commanded direction at the next available sample period since the target trajectories are stored in the data file at 20 Hz. The minimum time period between sets of radar dwells is restricted to 0.1 s (*i.e.*, 10 Hz). A set of radar dwells may consist of as many as five dwells that are requested simultaneously by the tracking algorithm. Each radar dwell requires 0.001 s of radar time to be accomplished. However, for the purposes of simulation, all of the dwells in a set are modeled as occurring at the same instant of time with respect to the target state. For a given detection threshold selected by the participant's radar management algorithm, the radar model will return, for each detection i of each dwell of the set, the following: the SNR $\Re_k^i$, bearing monopulse ratio r_k^{ib}, elevation monopulse ratio r_k^{ie}, and range r_k^i, where k denotes the dwell time, which is assumed to be equal for all dwells in the set. The sum and difference channels used to produce the angular measurements are corrupted with white Gaussian errors. Note that the errors in the monopulse ratio are not purely Gaussian.

Basic Radar Equation

The basic radar equation for a single pulse and target at range R is given in [19] as

$$P_r = \frac{P_t G_t G_r \lambda^2 F_t^2 F_r^2 \sigma_0}{(4\pi)^3 L_{tot}} \left(\frac{G_{stc}(R)}{R^4} \right) \tag{2.1}$$

where

P_r = Received power from the target

P_t = Transmitter power

G_t = Transmitter antenna gain in the direction of the target

G_r = Receiver antenna gain in the direction of the target

λ = Transmit wavelength

F_t = Transmitter propagation factor

F_r = Receiver propagation factor

σ_0 = Target RCS

L_{tot} = Total losses for the radar system

$G_{stc}(R)$ = Sensitivity Time Control (STC) gain

STC is employed to prevent saturation of the receiver by close-in scattering and to prevent short-range detection of objects with a small RCS. For this benchmark, the STC gain is defined as

$$G_{stc}(R) = \begin{cases} 1, & R \geq R_{stc} \\ \left(\dfrac{R}{R_{stc}}\right)^3, & R < R_{stc} \end{cases} \tag{2.2}$$

where $R_{stc} = 30$ km. The antenna gain along the boresight of the beam is computed in terms of the number of elements assuming half-wavelength separation distance between elements. Note that the gain becomes wavelength independent in this approximation. The effective aperture is given by

$$A_e = \varepsilon_A A \tag{2.3}$$

where ε_A is the aperture efficiency, and $A = L_x L_y$ is the actual area for array dimensions L_x and L_y. The gain is given by

$$\begin{aligned} G &= \frac{4\pi A_e}{\lambda^2} = \frac{4\pi\varepsilon_A}{\lambda^2} L_x L_y \\ &= \frac{4\pi\varepsilon_A}{\lambda^2}\left(\frac{N_x\lambda}{2}\frac{N_y\lambda}{2}\right) \\ &= \pi\varepsilon_A N_x N_y \end{aligned} \tag{2.4}$$

where N_x and N_y are the number of array elements in a particular dimension. In this benchmark, 55 elements per array side is assumed along with an aperture efficiency of 0.5. Thus, $G_t = G_r = 36.8$ dB for perfect beam pointing.

The noise power is given by

$$P_n = k_0 T_0 B_n F_n \tag{2.5}$$

where

k_0 = Boltzmann constant

T_0 = Reference temperature

B_n = Noise bandwidth

F_n = Receiver noise figure

The uncompressed (*i.e.*, no phase/frequency coding) SNR $\Re^u$ is given by

$$\Re^u = \frac{P_t G_t G_r \lambda^2 F_t^2 F_r^2 \sigma_0}{(4\pi)^3 L_{tot}} \left(\frac{1}{k_o T_0 B_n F_n}\right) \left(\frac{G_{stc}(R)}{R^4}\right) \tag{2.6}$$

For a radar with a given P_t, the SNR at the output of the matched filter can be increased by extending the length of the radar pulse. In order to achieve good range resolution with a long pulse, pulse compression is used. In discrete-coded pulse compression, the pulse width, τ_e, is composed of N_S subpulses of width τ_S (*i.e.*, $\tau_e = N_S \tau_S$), where each subpulse is coded with frequency and/or phase. For this benchmark problem, the radar waveform is biphase coded [18]. The subpulse width τ_S is assumed to be equal to the compressed pulse width τ_c and, thus, τ_S^{-1} defines the receiver bandwidth of the compressed pulse B_n. Modeling the compressed pulse as coherently integrated N_S subpulses, the output SNR for the compressed pulse is given by

$$\Re = \frac{P_t G_t G_r \lambda^2 F_t^2 F_r^2 \sigma_0}{(4\pi)^3 L_{tot}} \left(\frac{N_s \tau_c}{k_0 T_0 F_n}\right) \left(\frac{G_{stc}(R)}{R^4}\right) \tag{2.7}$$

Assuming an RCS of one square meter and the radar parameters of Table 2.1, the radar equation can be simplified to

$$\Re_0 = \tau_e \Omega_0 \left(\frac{G_{stc}(R)}{R^4}\right) \tag{2.8}$$

where $\Omega_0 = 257.6$ dB . For each of the eight waveforms and a one-square-meter target, the SNRs at 100 km were calculated using (2.8). The results are summarized in Table 2.2, where $\Delta r = 0.5 c \tau_S$ is the resolution of each pulse, with c being the speed of light.

The RCS of the target will be modeled as Swerling 3 type, where the density function for the RCS is given by

$$f(\sigma) = \frac{4\sigma}{\sigma_{ave}^2} \exp\left[-\frac{2\sigma}{\sigma_{ave}}\right] \tag{2.9}$$

with the average RCS (*i.e.*, σ_{ave}) varying between target scenarios. The cumulative distribution function of the radar cross section is given by

$$F(\sigma_0) = P\{0 \le \sigma \le \sigma_0\} = 1 - \left(1 + \frac{2\sigma_0}{\sigma_{ave}}\right) \exp\left[-\frac{2\sigma_0}{\sigma_{ave}}\right] \tag{2.10}$$

Table 2.1 Radar Parameters

P_t	1 MW (60 dBW)
G_t, G_r	4752 (36.8 dB)
λ	7.5 cm (−11.2 dB)
F_t, F_r	1 (0 dB)
L_{tot}	144.5 (21.6 dB)
k_0	1.38×10^{-23} J/K (−228.6 dB)
$(4\pi)^3$	1984.4 (33 dB)
T_0	290 K (24.6 dB)
F_n	2 (3 dB)

Table 2.2 Waveform Parameters

No.	τ_e (μs)	N_s	Δr (m)	$\Re_0$ @ 100 km (dB)
1	1.35	9	22.5	-1
2	2.25	15	22.5	1
3	4.05	27	22.5	3.7
4	5.85	39	22.5	5.3
5	11.70	78	22.5	8.3
6	23.40	156	22.5	11.3
7	46.8	78	90	14.3
8	93.6	156	90	17.3

Since $F(\sigma_0)$ is uniformly distributed between 0 and 1, a sample or observation of the RCS can be computed by solving

$$\left(1 + \frac{2\sigma_0}{\sigma_{ave}}\right) \exp\left[-\frac{2\sigma_0}{\sigma_{ave}}\right] = 1 - x \tag{2.11}$$

where x is a random number that is uniformly distributed between 0 and 1.

The power received from the SOJ is given by

$$P_{rj} = P_j G_{rj} \left(\frac{B_r}{B_j}\right) \tag{2.12}$$

where

P_j = Jammer power at the radar

G_{rj} = Radar receiver antenna gain in the direction of jammer

B_r = Effective bandwidth of the radar receive filters

B_j = Effective bandwidth of the jammer emission

For this benchmark, the SOJ power P_j will be a multiplicative factor of the noise power with $B_j > B_r$. Thus,

$$P_j = \gamma_0 \left(\frac{k_0 T_0 F_n}{\tau_c} \right) G_{rj} G_{stc}(R_{ctr}) \tag{2.13}$$

where $\gamma_0 = 8$ will be fixed during the benchmark, $G_{stc}(R_{ctr})$ is the STC gain evaluated at the center range bin of the active dwells and at unity on passive dwells.

Range Measurements

The range is computed as the range bin value that is closest to the true range in order to eliminate the need for processing adjacent bins for detection. Also, since the targets are assumed to be points in space and no interpolation between bins is performed, the discrete coding results in range measurements with errors that are uniformly distributed and defined by the bin resolution (*i.e.*, independent of SNR).

The center of the range gate is placed at the predicted range $\hat{r}_k$ provided by the tracking algorithm. The range measurement is computed as follows. The prediction error in range is given by

$$\tilde{r}_k = R_k^t - \hat{r}_k \tag{2.14}$$

where R_k^t is the true range of the target at time k. If $|\tilde{r}_k| > 775$ m, then a missed detection occurs and none of the measurements that are returned will include the target. If the target is in the range gate, the range measurement is given by

$$r_k = \Delta r \ \mathrm{rd}\left[\frac{\tilde{r}_k}{\Delta r} \right] + \hat{r}_k \tag{2.15}$$

where Δr is specified in Table 2.2 for each waveform and rd[·] denotes the nearest integer. The range of an FA is assigned to that range of the bin in which it occurs.

Antenna Gain Patterns

The array consists of 3025 individual elements (*i.e.*, 55 elements in elevation and bearing) with cosine illumination and half-power beamwidth of 140°. The broadside of the array is directed at 0° bearing and 15° elevation. The normalized voltage patterns [20] are defined by $V_e(E_k^t, \hat{e}_k)$, the voltage pattern in elevation pointed at $\hat{e}_k$ and target at E_k^t, and $V_b(B_k^t, \hat{b}_k)$, the voltage pattern in bearing pointed at $\hat{b}_k$ and target at B_k^t, and are given by

$$V_e(E_k^t, \hat{e}_k) = \frac{\pi}{4(1.43)} \frac{\sin(Nb_2)}{N\sin(b_2)} \left[\frac{\sin(b_1 + 0.5\pi)}{b_1 + 0.5\pi} + \frac{\sin(b_1 - 0.5\pi)}{b_1 - 0.5\pi} \right] \tag{2.16}$$

$$V_b(B_k^i, \hat{b}_k) = \frac{\pi}{4(1.43)} \frac{\sin(Na_2)}{N\sin(a_2)} \left[\frac{\sin(a_1 + 0.5\pi)}{a_1 + 0.5\pi} + \frac{\sin(a_1 - 0.5\pi)}{a_1 - 0.5\pi} \right] \tag{2.17}$$

where

$$a_1 = 0.25 \sin(B_k^i) \tag{2.18}$$

$$a_2 = 0.5\pi \left[\sin(B_k^i) - \sin(\hat{b}_k) \right] \tag{2.19}$$

$$b_1 = 0.25 \sin(E_k^i - e_b) \tag{2.20}$$

$$b_2 = 0.5\pi \left[\sin(E_k^i - e_b) - \sin(\hat{e}_k - e_b) \right] \tag{2.21}$$

$$N = 55 \tag{2.22}$$

$$e_b = 15^\circ \tag{2.23}$$

The factor of 1.43 has been included to give a normalized sum channel voltage at boresight for a broadside angle of 0°.

Channel Voltages

The received voltage will be related to the received power as $V_r = \sqrt{2P_r}$. In search or track mode, the sum voltage at time k, s_k, is composed of the in-phase and quadrature portions. The in-phase and quadrature components of the sum voltage s'_k normalized by the receiver noise is given by

$$s'_{Ik} = \Gamma_k^i (\Sigma_k^i)^2 \cos\phi_k^i + \Gamma_k^j \Sigma_k^j \cos\phi_k^j + N(0,1) \tag{2.24}$$

$$s'_{Qk} = \Gamma_k^i (\Sigma_k^i)^2 \sin\phi_k^i + \Gamma_k^j \Sigma_k^j \sin\phi_k^j + N(0,1) \tag{2.25}$$

where

$$\Gamma_k^i = \frac{\mathcal{K}_0}{(R_k^i)^2} \sqrt{\tau_e \sigma_0 G_{stc}(R_k^i)} \tag{2.26}$$

$$\Gamma_k^j = \sqrt{\gamma_0 G_{stc}(R_k^i) \left[N^2(0,1) + N^2(0,1) \right]} \tag{2.27}$$

$$\mathcal{K}_0 = \sqrt{\frac{2P_t G^2 \lambda^2}{(4\pi)^3 L_{tot} k_0 T_0 F_n}} = \sqrt{2\Omega_0} = 130.2 \text{ dB} \tag{2.28}$$

$$\Sigma_k^i = \Psi_k^i(\theta_{sq}^a, \theta_{sq}^b) + \Psi_k^i(-\theta_{sq}^a, \theta_{sq}^b) + \Psi_k^i(\theta_{sq}^a, -\theta_{sq}^b) + \Psi_k^i(-\theta_{sq}^a, -\theta_{sq}^b) \tag{2.29}$$

$$\Sigma_k^j = \Psi_k^j(\theta_{sq}^a, \theta_{sq}^b) + \Psi_k^j(-\theta_{sq}^a, \theta_{sq}^b) + \Psi_k^j(\theta_{sq}^a, -\theta_{sq}^b) + \Psi_k^j(-\theta_{sq}^a, -\theta_{sq}^b) \tag{2.30}$$

$$\Psi_k^i(x,y) = \left[V_a(E_k^i, \hat{e}_k + x) V_b(B_k^i, \hat{b}_k + y) \right] \tag{2.31}$$

$$\Psi_k^j(x,y) = \left[V_a(E_k^j, \hat{e}_k + x) V_b(B_k^j, \hat{b}_k + y) \right] \tag{2.32}$$

$$\theta^e_{sq} = \theta_{sq0}/\cos(\hat{e}_k - e_k) \tag{2.33}$$

$$\theta^b_{sq} = \theta_{sq0}/\cos(\hat{b}_k) \tag{2.34}$$

τ_c = Pulse length

ϕ^t_k = Phase of the voltage of the target return

ϕ^j_k = Phase of the voltage of the SOJ

B^j_k = Bearing of the SOJ at time k

E^j_k = Elevation of the SOJ at time k

Both ϕ^t_k and ϕ^j_k are independent and uniformly distributed between 0 and 2π. The θ^e_{sq} and θ^b_{sq} denote the squint angles[6] in elevation and bearing, respectively, where $\theta_{sq0} = 0.9° = 15.7$ mrad. Also, $N(0,1)$ denotes a Gaussian random variable with zero mean and unity variance. Let

$$(s'_k)^2 = (s'_{Ik})^2 + (s'_{Qk})^2 \tag{2.35}$$

Then the observed SNR is computed by $\Re_k = 0.5(s'_k)^2$.

Eqs. (2.24) through (2.34) are used to compute a measurement for each range bin by setting $\Gamma^i_k = 0$ for the bins that do not include the target. The passive measurements are obtained by setting $\Gamma^i_k = 0$ and $G_{stc} = 1$ for all range bins. The observed SNR $\Re^i_k$ and range r^i_k are returned for every range bin i with $\Re^i_k > \Re^{ih}_k$, where $\Re^{ih}_k$ is specified by the tracking algorithm for the dwell set at time k. In other words, a measurement is returned for range bin i if $\Re^i_k > \Re^{ih}_k$. Thus, the probability of an FA P_{fa} is specified by the tracking algorithm. The amplitudes of the FAs are Rayleigh distributed with parameter $\gamma_0(\Sigma^j_k)^2 G_{stc}(R) + 1$. Since the passive measurements are obtained by setting $\Gamma^i_k = 0$ and $G_{stc} = 1$ for all range bins, the amplitude of the measurements of a pass dwell will be Rayleigh distributed with parameter $\gamma_0(\Sigma^j_k)^2 + 1$.

Figure 2.1 shows the one-way beamwidth θ_{BW} of the sum channel versus the off-broadside angle, which is the angle between the boresight of the beam and a vector orthogonal (*i.e.*, normal) to the face of the array. The broadside angle is treated independently in elevation and bearing. The one-way beamwidth is the angle between the two half-power points on the sum channel beam. The one-way beamwidth varies from 2.4° at broadside to 4.5° at a broadside angle of 60°. The two-way beamwidth varies from 1.6° at broadside to 3.2° at a broadside angle of 60°. Figure 2.2 shows the normalized antenna gain versus the off-broadside

[6] Note that the squint angles are usually fixed with respect to the off-broadside angle. The squint angles have been varied with the off-broadside angle to increase the minimum monopulse error slope.

angle, where the gain has been normalized by the gain at broadside. Thus, antenna gains G_t and G_r are decreased by 0.4 dB at a broadside angle of 60°.

The difference voltages in elevation d_k^e and bearing d_k^b have in-phase and quadrature components. The in-phase and quadrature components of d_k^e and d_k^b are written as

$$d_{Ik}^e = \Gamma_k^i \Sigma_k^i \left[\Psi_k^i(\theta_{sq}^e, \theta_{sq}^b) + \Psi_k^i(\theta_{sq}^e, -\theta_{sq}^b) - \Psi_k^i(-\theta_{sq}^e, \theta_{sq}^b) - \Psi_k^i(-\theta_{sq}^e, -\theta_{sq}^b) \right] \cos\phi_k^i + \Gamma_k^j \left[\Psi_k^j(\theta_{sq}^e, \theta_{sq}^b) + \Psi_k^j(\theta_{sq}^e, -\theta_{sq}^b) - \Psi_k^j(-\theta_{sq}^e, \theta_{sq}^b) - \Psi_k^j(-\theta_{sq}^e, -\theta_{sq}^b) \right] \cos\phi_k^j + N(0,1) \quad (2.36)$$

$$d_{Qk}^e = \Gamma_k^i \Sigma_k^i \left[\Psi_k^i(\theta_{sq}^e, \theta_{sq}^b) + \Psi_k^i(\theta_{sq}^e, -\theta_{sq}^b) - \Psi_k^i(-\theta_{sq}^e, \theta_{sq}^b) - \Psi_k^i(-\theta_{sq}^e, -\theta_{sq}^b) \right] \sin\phi_k^i + \Gamma_k^j \left[\Psi_k^j(\theta_{sq}^e, \theta_{sq}^b) + \Psi_k^j(\theta_{sq}^e, -\theta_{sq}^b) - \Psi_k^j(-\theta_{sq}^e, \theta_{sq}^b) - \Psi_k^j(-\theta_{sq}^e, -\theta_{sq}^b) \right] \sin\phi_k^j + N(0,1) \quad (2.37)$$

$$d_{Ik}^b = \Gamma_k^i \Sigma_k^i \left[\Psi_k^i(\theta_{sq}^e, \theta_{sq}^b) + \Psi_k^i(-\theta_{sq}^e, \theta_{sq}^b) - \Psi_k^i(\theta_{sq}^e, -\theta_{sq}^b) - \Psi_k^i(-\theta_{sq}^e, -\theta_{sq}^b) \right] \cos\phi_k^i + \Gamma_k^j \left[\Psi_k^j(\theta_{sq}^e, \theta_{sq}^b) + \Psi_k^j(-\theta_{sq}^e, \theta_{sq}^b) - \Psi_k^j(\theta_{sq}^e, -\theta_{sq}^b) - \Psi_k^j(-\theta_{sq}^e, -\theta_{sq}^b) \right] \cos\phi_k^j + N(0,1) \quad (2.38)$$

$$d_{Qk}^b = \Gamma_k^i \Sigma_k^i \left[\Psi_k^i(\theta_{sq}^e, \theta_{sq}^b) + \Psi_k^i(-\theta_{sq}^e, \theta_{sq}^b) - \Psi_k^i(\theta_{sq}^e, -\theta_{sq}^b) - \Psi_k^i(-\theta_{sq}^e, -\theta_{sq}^b) \right] \sin\phi_k^i + \Gamma_k^j \left[\Psi_k^j(\theta_{sq}^e, \theta_{sq}^b) + \Psi_k^j(-\theta_{sq}^e, \theta_{sq}^b) - \Psi_k^j(\theta_{sq}^e, -\theta_{sq}^b) - \Psi_k^j(-\theta_{sq}^e, -\theta_{sq}^b) \right] \sin\phi_k^j + N(0,1) \quad (2.39)$$

where the received errors in the difference channels have been modeled as independent of the receiver errors in the sum channel. Passive measurements are generated by setting $\Gamma_k^i = 0$.

Monopulse Processing

Monopulse processing is a simultaneous lobing technique for determining the angular location of a source of radiation or of a "target" that reflects part of the energy incident upon it [21]. The monopulse ratio is formed by the (complex) division of the difference-channel voltage phasor by the sum-channel voltage phasor. Monopulse ratios are formed separately for the elevation and bearing directions of arrival. For every active or passive track dwell, monopulse ratios are returned for every measurement with an amplitude that exceeds the specified detection threshold $\Re_k^{th}$. The monopulse ratios are then used to estimate the monopulse error function value η for determining the measured direction of arrival. The processing of monopulse ratios will be considered as in Appendix A for (i) target only measurements, (ii) SOJ only, and (iii) target in the presence of the SOJ within the mainlobe of the antenna pattern.

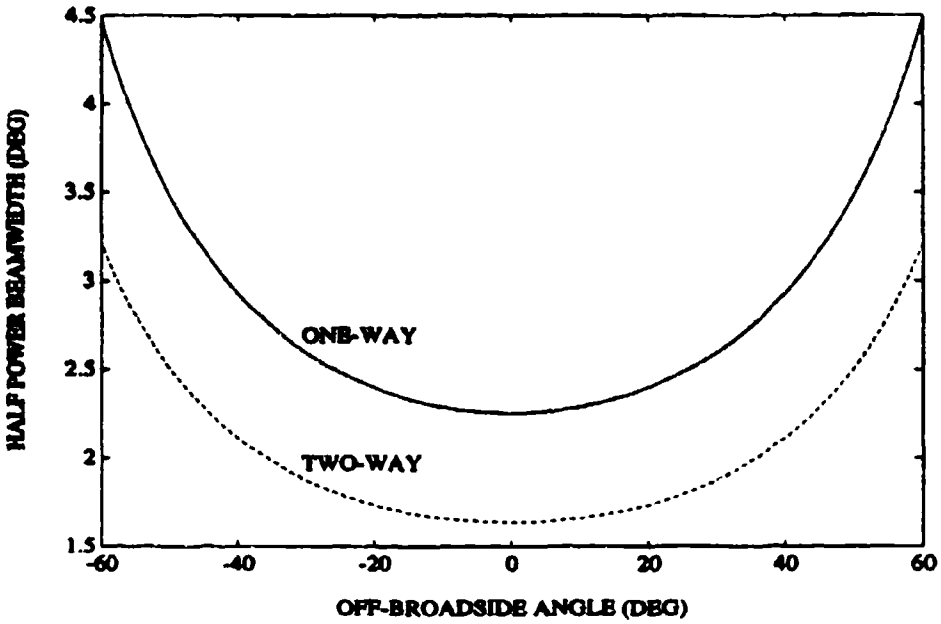

Figure 2.1 Beamwidth Versus Off-Broadside Angle

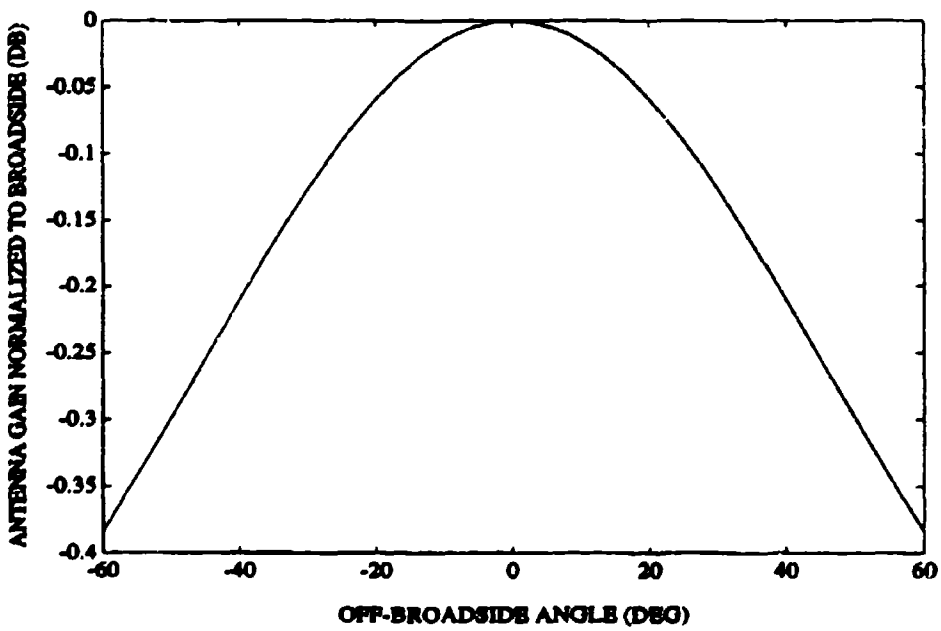

Figure 2.2 Normalized Antenna Gain Versus Off-Broadside Angle

The monopulse error function at broadside is shown in Figure 2.3 along with the commonly used linear approximation to the monopulse error function, which is given by

$$\eta \approx k_m \theta, \qquad -\theta_{BW} < \theta < \theta_{BW} \tag{2.40}$$

where k_m is the average monopulse error slope for $-0.5\ \theta_{BW} < \theta < 0.5\ \theta_{BW}$. Figure 2.4 shows the monopulse error slopes versus the off-broadside angle. Since the squint angles are increased with the broadside angle, the monopulse error slope k_m achieves a minimum of 24 rad^{-1} rather than 12 rad^{-1} if the squint angles had been fixed at their boresight values. Since the standard deviations of the angle measurements are inversely proportional to k_m, maintaining a higher k_m provides more accurate measurements at the off-broadside angles.

The monopulse ratios in elevation and bearing are computed as

$$r_k^e = \frac{s'_{Ik} d^e_{Ik} + s'_{Qk} d^e_{Qk}}{(s'_{Ik})^2 + (s'_{Qk})^2} \tag{2.41}$$

$$r_k^b = \frac{s'_{Ik} d^b_{Ik} + s'_{Qk} d^b_{Qk}}{(s'_{Ik})^2 + (s'_{Qk})^2} \tag{2.42}$$

When detecting a single target, the Directions-Of-Arrival (DOA) estimates in elevation η_k^{te} and bearing η_k^{tb} are given by

$$\hat{\eta}_k^{te} = \left(1 + \frac{1}{2\Re_k}\right) r_k^e, \qquad \Re_k > 3 \text{ dB} \tag{2.43}$$

$$\hat{\eta}_k^{tb} = \left(1 + \frac{1}{2\Re_k}\right) r_k^b, \qquad \Re_k > 3 \text{ dB} \tag{2.44}$$

Using the linear approximation for the monopulse error function gives the measurements of elevation and bearing as

$$e_k^t = \hat{e}_k + \frac{\hat{\eta}_k^{te}}{k_m^e} \tag{2.45}$$

$$b_k^t = \hat{b}_k + \frac{\hat{\eta}_k^{tb}}{k_m^b} \tag{2.46}$$

where

$$k_m^e = 48\, cos(\hat{e}_k - e_b) \qquad \frac{\text{volt}}{\text{volt} \cdot \text{rad}} \tag{2.47}$$

$$k_m^b = 48\, cos(\hat{b}_k) \qquad \frac{\text{volt}}{\text{volt} \cdot \text{rad}} \tag{2.48}$$

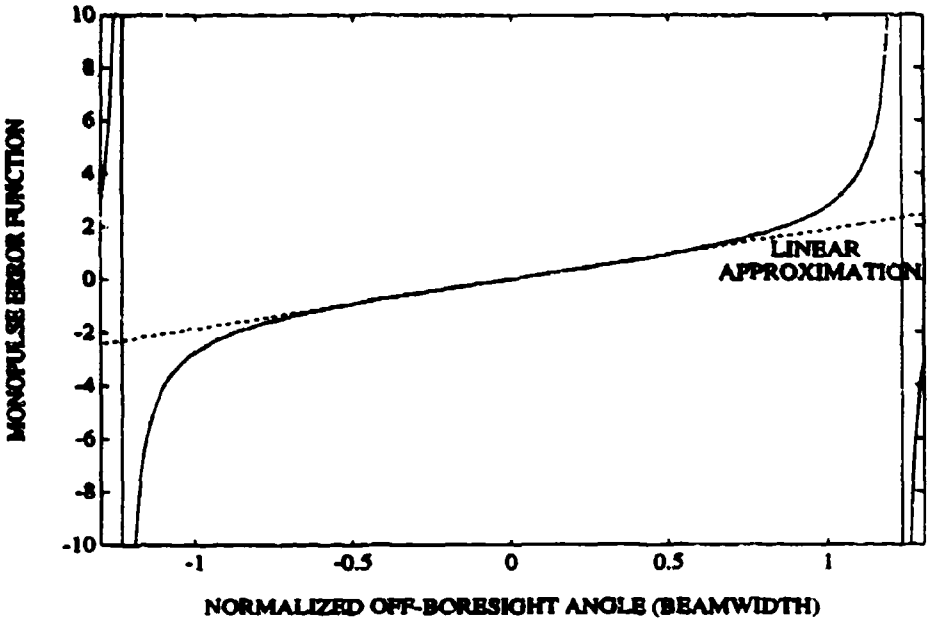

Figure 2.3 Monopulse Error Function at Broadside

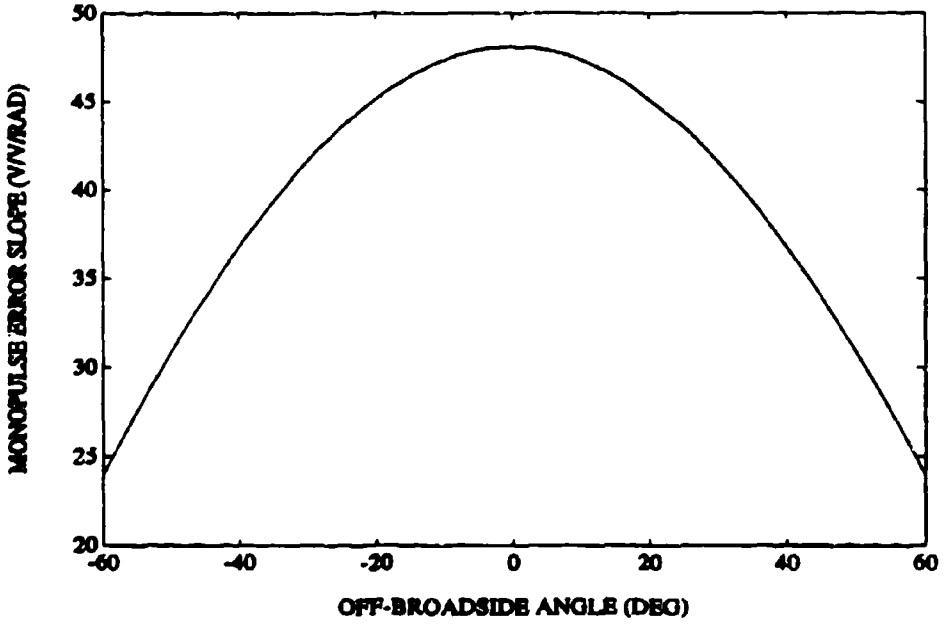

Figure 2.4 Monopulse Error Slopes Versus Off-Broadside Angle

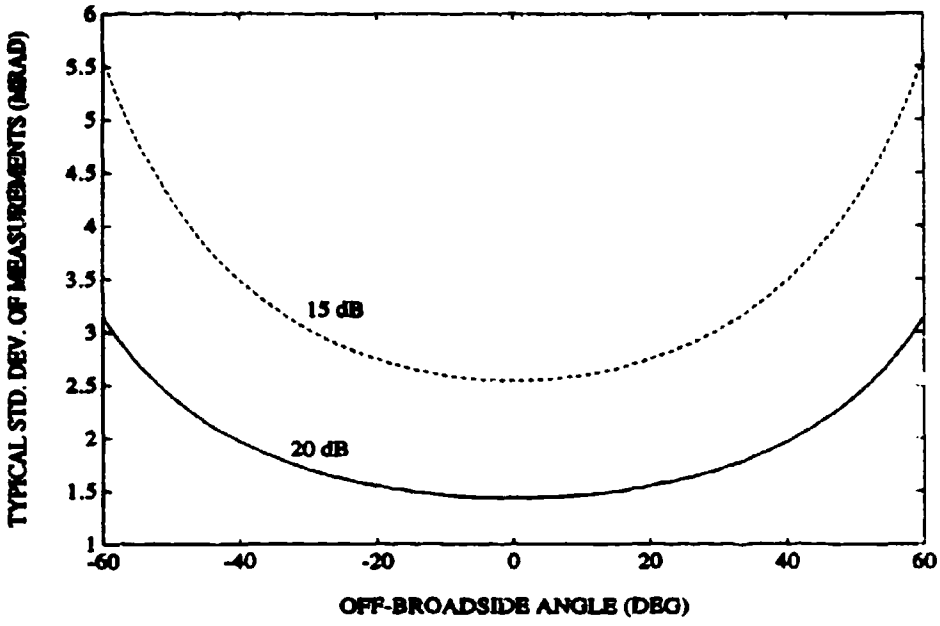

Figure 2.5 Typical Standard Deviations of the Measurements

and $\hat{e}_k$ and $\hat{b}_k$ are the elevation and bearing pointing commands from the tracking algorithm. Estimates for the standard deviations of the measurements are given by

$$\hat{\sigma}_k^{te} = \frac{1}{k_m^e \sqrt{2\Re_k}} \left[1 + \frac{1}{2\Re_k}\right] \left[1 + \frac{(r_k^e)^2}{4\Re_k}\right]^{0.5}, \qquad \Re_k > 3 \text{ dB} \tag{2.49}$$

$$\hat{\sigma}_k^{tb} = \frac{1}{k_m^b \sqrt{2\Re_k}} \left[1 + \frac{1}{2\Re_k}\right] \left[1 + \frac{(r_k^b)^2}{4\Re_k}\right]^{0.5}, \qquad \Re_k > 3 \text{ dB} \tag{2.50}$$

Note that (2.49) and (2.50) differ from the expression given in [21] for the standard deviation. The variance expression in [21] is based on an assumption of $|\eta| \ll 1$ and $\Re_k > 12$ dB, while (2.49) and (2.50) are valid for $|\eta| < 2$ and $\Re_k > 3$ dB. Figure 2.5 gives the standard deviation for various off-broadside steering angles and $\Re_k = 15$ and 20 dB with perfect pointing (*i.e.*, $d_k^b = 0$). Note that $\Re_k$ can vary rather significantly between consecutive measurements since the targets have a RCS of Swerling 3 type.

When processing the passive measurements of the SOJ, the Jammer-to-Noise Ratio (JNR) J_k can be estimated from N detections within a dwell according to

$$\hat{J}_k = -1 + \frac{1}{N} \sum_{i=1}^{N} \Re_k^i \tag{2.51}$$

where $\Re_k^i$ is the observed SNR of the range bin i at time k. The DOA estimates for the elevation and bearing of the SOJ are given by

$$\hat{\eta}_k^{je} = \left[1 + \frac{1}{\hat{J}_k}\right] \hat{r}_k^{je}, \qquad \hat{J} > 3 \text{ dB} \tag{2.52}$$

$$\hat{\eta}_k^{jb} = \left[1 + \frac{1}{\hat{J}_k}\right] \hat{r}_k^{jb}, \qquad \hat{J}_k > 3 \text{ dB} \tag{2.53}$$

where

$$\hat{r}_k^{je} = \frac{\sum_{i=1}^{N} \Re_k^i r_k^{ie}}{\sum_{n=1}^{N} \Re_k^n} \tag{2.54}$$

$$\hat{r}_k^{jb} = \frac{\sum_{i=1}^{N} \Re_k^i r_k^{ib}}{\sum_{n=1}^{N} \Re_k^n} \tag{2.53}$$

with r_k^{ie} and r_k^{ib} denoting the monopulse ratio for range bin i at time k for the elevation and bearing, respectively. The $\hat{r}_k^{je}$ and $\hat{r}_k^{jb}$ are the minimum variance estimates of the means of the monopulse ratios for elevation and bearing, respectively. Using (2.52) and (2.53) in (2.45) and (2.46) provides the measured elevation and bearing of the SOJ. Estimates for the standard deviations of the SOJ measurements are given by

$$\hat{\sigma}_k^{je} = \frac{1}{\sqrt{2k_m^e}} \left[\sum_{i=1}^{N} \Re_k^i\right]^{-0.5} \left[1 + \frac{1}{\hat{J}_k}\right] \left[1 + \left(1 + \frac{1}{\hat{J}_k}\right)(\hat{r}_k^{je})^2\right]^{0.5}, \qquad \hat{J}_k > 3 \text{ dB} \tag{2.56}$$

$$\hat{\sigma}_k^{jb} = \frac{1}{\sqrt{2k_m^b}} \left[\sum_{i=1}^{N} \Re_k^i\right]^{-0.5} \left[1 + \frac{1}{\hat{J}_k}\right] \left[1 + \left(1 + \frac{1}{\hat{J}_k}\right)(\hat{r}_k^{jb})^2\right]^{0.5}, \qquad \hat{J}_k > 3 \text{ dB} \tag{2.57}$$

When the target and the SOJ are in the mainlobe of the antenna pattern, the angular location of the SOJ can be observed as discussed in (2.51) through (2.57) with a passive dwell or an active dwell, where only the range bins that do not include the target are to be considered. Thus, the DOA estimates for the target in the presence of the SOJ in the mainlobe are given by

$$\hat{\eta}_k^{t|je} = \left[1 + \frac{J_k + 1}{2\Re_k}\right] r_k^e - \left[\frac{\hat{J}_k + 1}{2\Re_k}\right] \hat{r}_k^{je}, \qquad \Re_k > 2J_k + 2 \tag{2.58}$$

$$\hat{\eta}_k^{t|jb} = \left[1 + \frac{J_k + 1}{2\Re_k}\right] r_k^b - \left[\frac{\hat{J}_k + 1}{2\Re_k}\right] \hat{r}_k^{jb}, \qquad \Re_k > 2J_k + 2 \tag{2.59}$$

where $\hat{r}_k^{je}$ and $\hat{r}_k^{jb}$ are the minimum variance estimates of the means of the monopulse ratios that do not include the target. Eqs. (2.58) and (2.59) indicate that if the observed SNR $\Re_k$ is

12 dB greater than the JNR J_k, the effects of the SOJ can be ignored. Note that J_k should be estimated on the active dwell since the SOJ power can fluctuate between consecutive radar dwells. Using (2.58) and (2.59) in (2.45) and (2.46) provides the measured elevation and bearing of the target in the presence of the jammer. Estimates of the standard deviations of the measurements are given by

$$\sigma_k^{tj^e} = \frac{1}{k_m^e\sqrt{2\Re_k}}\left[1+\frac{\widehat{J}_k+1}{2\Re_k}\right]\left[1+\left(1+\frac{1}{\widehat{J}_k}\right)(\hat{r}_k^{j^e})^2+\left(r_k^e-\hat{r}_k^{j^e}\right)^2\left(\frac{(\widehat{J}_k+1)^2}{2\Re_k}\right)\right]^{0.5} \quad (2.60)$$

$$\sigma_k^{tj^b} = \frac{1}{k_m^b\sqrt{2\Re_k}}\left[1+\frac{\widehat{J}_k+1}{2\Re_k}\right]\left[1+\left(1+\frac{1}{\widehat{J}_k}\right)(\hat{r}_k^{j^b})^2+\left(r_k^b-\hat{r}_k^{j^b}\right)^2\left(\frac{(\widehat{J}_k+1)^2}{2\Re_k}\right)\right]^{0.5} \quad (2.61)$$

where $\Re_k > 2\widehat{J}_k + 2$. Eqs. (2.58) and 2.59) provide estimates of the DOAs of a target in the presence of an SOJ and (2.60) and (2.61) provide estimates of the variance associated with the DOA estimates. However, note that η_j and J have been used as known quantities. Then a sufficiently large number of range bins should be used to estimate J and η_j. A reasonable criteria for M is $M\widehat{J} > 18$ dB. For example, an SOJ with $J = 6$ dB would require about 16 range bins.

CHAPTER 3
ECM TECHNIQUES AND MODELING

The ECM for the benchmark involves the SOJ discussed in Chapter 2 and RGPO. The times at which the SOJ and RGPO impact the trajectories are discussed in the next section. The SOJ transmits broadband noise toward the radar and has the effect of increasing the level of noise. However, since the SOJ noise enters the sum and difference channels with the same phase, the DOA of the SOJ can be estimated with the monopulse ratios, where the target amplitude is Rayleigh, since the SOJ noise is modeled as Gaussian. The SOJ flies an oval (race course) holding pattern in a clockwise direction at an altitude of 3.05 km and speed of 168 m/s. The SOJ is approximately 150 km from the radar, and its trajectory is shown in Figure 3.1. The aircraft flies straight and level for a period of approximately 40 s, upon which a 1.0-g turn is performed through a 180-degree heading change. Straight and level, nonaccelerating flight is continued for another 40 s, where a second 1.0-g turn is performed until the aircraft returns to its original position. Then the cycle starts again with another 40 s of level flight maintained. The SOJ transmits broadband noise that impacts the radar with power no more than γ_0 times the receiver noise power, as discussed in Chapter 2. For this benchmark, $\gamma_0 = 8$. Thus, the SOJ will not completely hide a target and it can be defeated with a higher energy waveform in this benchmark. While the SOJ energy enters into every radar dwell, the effects of the SOJ are, for the most part, negligible when it is not in the mainlobe of the antenna pattern. Note that this is not the case for SOJs transmitting a higher level of power.

In RGPO, the target under track repeats, with delay and amplification, the radar pulse so as to pull the radar range gate off the target. The time delay is controlled so that the false target is separated from the target with linear or quadratic motion. For the linear case, the range of the false target with respect to the radar is expressed as

$$R_k^{ft} = R_k^t + v_{po}(t_k - t_0) \tag{3.1}$$

where R_k^t is the range of the actual target, v_{po} is the rate of pull-off, t_k is the time of the radar dwell, and t_0 is the initial reference time of the RGPO false target. For the quadratic

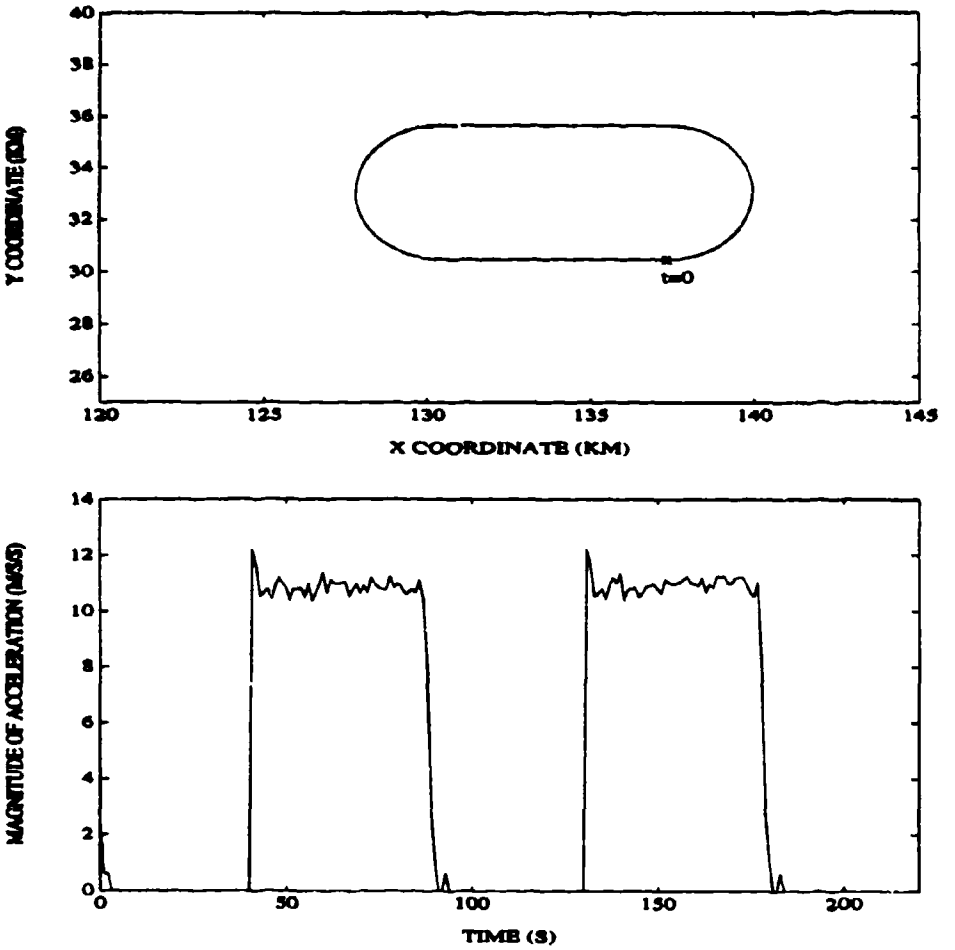

Figure 3.1 Trajectory for SOJ

case, the range of the false target with respect to the radar is written as

$$R_k^{ft} = R_k^t + \frac{1}{2}a_{po}(t_k - t_0)^2 \tag{3.2}$$

where a_{po} is the acceleration of pull-off of the false target. The measurements of the RGPO will be generated as those for the target with (2.26) modified according to

$$\Gamma_k^{ft} = \frac{\mathcal{K}_0}{(R_k^t)^2}\sqrt{\tau_e \gamma_1 \sigma_{ave} G_{stc}(R_k^t)} \tag{3.3}$$

where γ_1 is the amplification factor of the RGPO. However, when the times of arrival of the target echo and the false target are less than the resolution of the radar, interference occurs. For this benchmark, two returns are assumed to be resolved when their times of arrival differ

by more than $\frac{\tau_e}{3}$. Thus, if

$$\frac{6|R_k^{ft} - R_k^t|}{c\,\tau_e} < 1 \tag{3.4}$$

the target and RGPO amplitudes are modified according to

$$\Gamma_k^t = \Gamma_k^t + \left[1 - \frac{6|R_k^{ft} - R_k^t|}{c\,\tau_e}\right] \Gamma_k^{ft} \cos(2\pi\epsilon_k) \tag{3.5}$$

$$\Gamma_k^{ft} = \Gamma_k^{ft} + \left[1 - \frac{6|R_k^{ft} - R_k^t|}{c\,\tau_e}\right] \Gamma_k^t \cos(2\pi\epsilon_k) \tag{3.6}$$

where $\epsilon_k = \phi_k^t - \phi_k^{ft}$ with ϕ_k^{ft} being the phase of the false target signal, and c is the speed of light. Note that the discrete coding of phase has been largely neglected in the modeling of the interference of the two returns.

The RGPO is activated by a radar dwell on the target. Thus, RGPO reference times are dependent on the dwell times of the radar. For the benchmark, RGPO will be activated on the next pulse after a time specified in the trajectory file. The reference time t_0 will be chosen as the dwell time t_k minus a uniformly distributed random number between 0.1 and 0.5 μs. Thus, $t_k - t_0$ will be uniformly distributed between 0.1 and 0.5 μs. The amplification factor γ_1 is chosen as a uniformly distributed number between 1 and 4. The rates for both modes have been selected to yield a 2 km displacement in range of the false target in 20 s. Thus, the pull-off rates are $v_{po} = 100$ m/s and $a_{po} = 10$ m/s^2.

Cover pulse is a RGPO technique that uses echoes without the waveform coding and attempts to cover the actual target return. When cover pulse is used, a noncoherent detection occurs. Typically the range resolution of the noncoherent detection is rather bad. For this benchmark, cover pulse is not considered.

CHAPTER 4

TARGET TRAJECTORIES

The targets will exhibit RCS fluctuations according to the Swerling 3 type model and perform as much as 7 g of lateral acceleration and 2 g of longitudinal acceleration. Target range can vary from 20 to 120 km, while the target elevation angle varies from 2° to 80°. Since only one radar face is used, the bearing of the target will be confined to ±60°. The average RCSs of the targets are large enough so that average SNRs of 18 dB are achievable with the highest energy waveform. The SOJ remains at ranges greater than 150 km and performs less than 2 g of acceleration. The RGPO can be employed only when the angle between the target heading vector and radar range vector is within 180° ± 60°. While six target trajectories are specified in this section, the tracking algorithm should be designed to handle targets satisfying these general specifications.

The first target trajectory is shown in Figure 4.1 and represents a large aircraft, such as a military cargo aircraft. From an initial range of 80 km, the target flies on a constant course with a speed of 290 m/s at an altitude of 1.26 km for the first minute. The aircraft then performs a mild 2-g turn and continues on the new course for a period of 30 s, where a 3-g turn is made, and the aircraft flies away from the radar to a final range of 70 km. The σ_{ave} is 4 m^2, RGPO starts after 15 and 40 s, and the SOJ is within 2 degrees of the target Line-of-Sight (LOS) from 82 to 93 s.

The second target trajectory is shown in Figure 4.2 and represents a trajectory that would be expected by a smaller, more maneuverable aircraft, such as a Learjet or other similar high-performance commercial aircraft. Target 2 initializes at a range of 63 km, a speed of 305 m/s, and an altitude of 4.57 km. The target performs a 2.5-g turn through 90 degrees of course change. After the turn, the target then descends gradually to an altitude of approximately 3.05 km. A 4-g turn rolling out to straight and level flight is performed at a constant speed of 305 m/s, and the trajectory ends near a range of 28 km. The σ_{ave} is 2 m^2; RGPO starts after 12, 50, and 95 s; and the SOJ does not approach the target LOS.

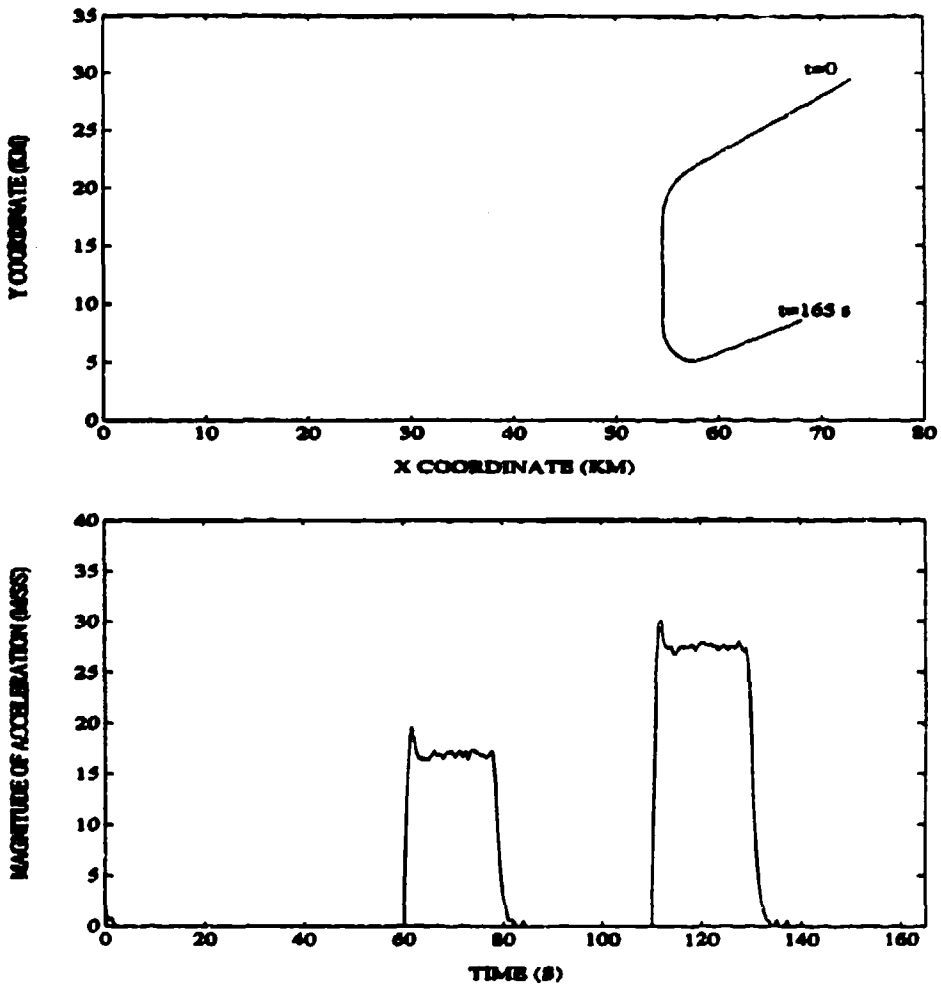

Figure 4.1 Trajectory for Target 1

The trajectories of Targets 3 and 4 are shown in Figures 4.3 and 4.4 and represent medium bombers flying at high speeds with good maneuverability. Target 3 has an initial speed of 457 m/s and flies straight and level for the first 30 s. A 4-g turn is then performed through a 45-degree course change. Straight and level, nonaccelerating flight is continued for the next 30 s. A second 4-g turn through a 90-degree course change to straight and level flight is performed while the aircraft decelerates to a speed of 274 m/s. The σ_{rcs} is 1.5 m^2; RGPO starts after 30, 100, and 130 s; and the SOJ does not approach the target LOS. Target 4 maintains a speed of 251 m/s and an altitude of 2.29 km for the first 30 s. A 4-g turn is performed through a course change of 45 degrees. After another 30 s, a 6-g turn is performed as the throttle is increased to full afterburner. The aircraft pitches up and climbs to an altitude of 4.57 km. Following the climb, straight and level, nonaccelerating flight is maintained for the

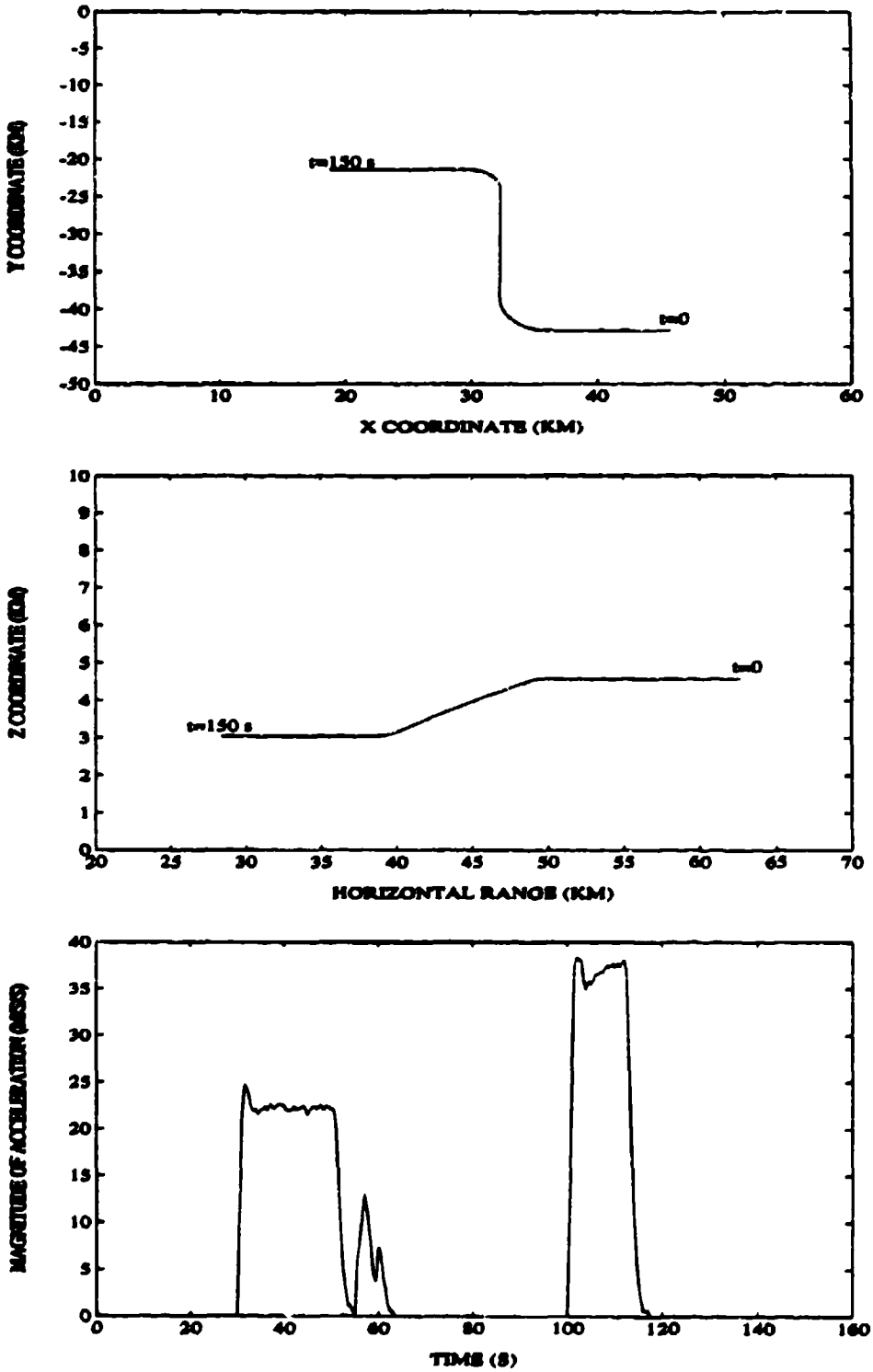

Figure 4.2 Trajectory for Target 2

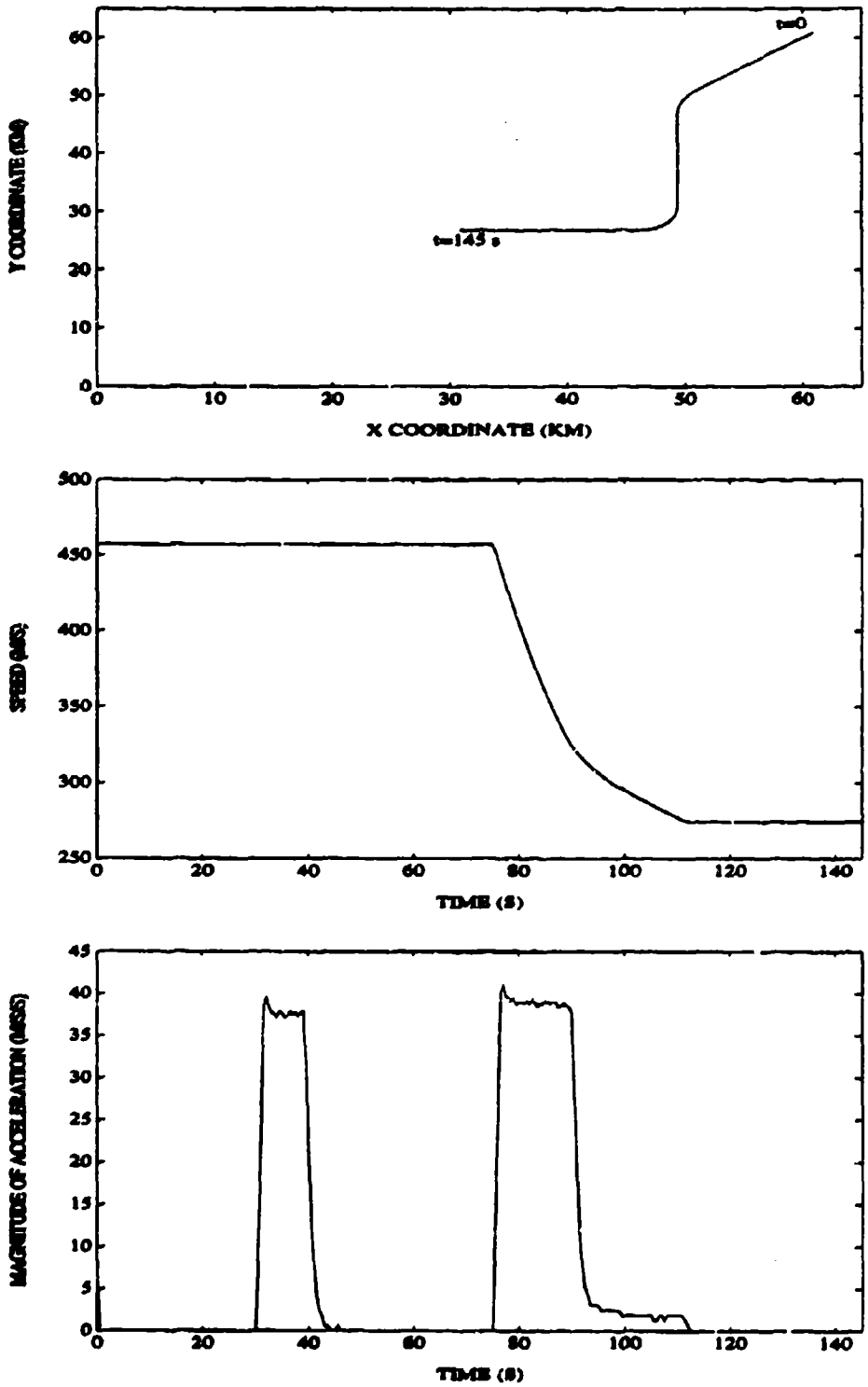

Figure 4.3 Trajectory for Target 3

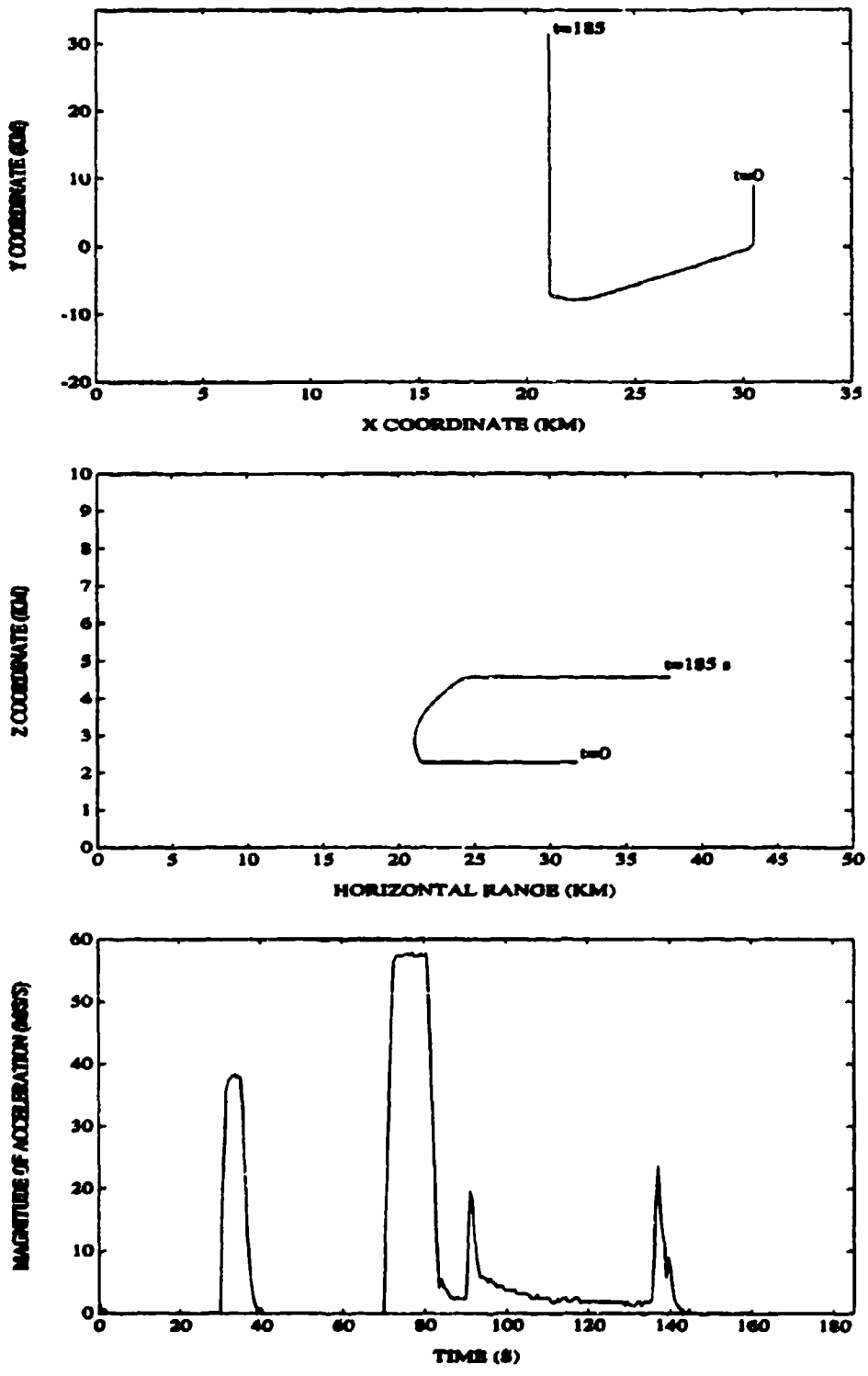

Figure 4.4 Trajectory for Target 4

completion of the trajectory. The σ_{ave} is 1.7 m^2, RGPO starts after 35 and 65 s, and the SOJ is within 2 degrees of the target LOS from 5 to 12 s and 118 to 122 s.

Targets 5 and 6 are shown in Figures 4.5 and 4.6 and represent fighter/attack aircraft. Target 5 is initialized in a thrusting acceleration at an altitude of 1.5 km. After a period of 30 s, a 5-g turn is performed while maintaining full throttle. This turn is followed 20 s later by a 7-g turn. Following the second turn, straight and level, nonaccelerating flight is performed for 30 s, upon which a 6-g turn is performed concurrently with a pitch up and a climb. After an altitude of 4.45 km is reached, straight and level, nonaccelerating flight is flown for the completion of the trajectory. The σ_{ave} is 1.2 m^2; RGPO starts after 5, 25, and 52 s; and the SOJ is within 2 degrees of the target LOS from 75 to 83 s. Target 6 starts at a speed of 426 m/s and an altitude of 1.55 km. Constant speed and course are maintained for a period of 30 s upon which a 7-g turn is performed. The new course is maintained for another 30 s. A 6-g turn is performed while the throttle is reduced and the aircraft is nosed over in order to decrease altitude. After a final altitude of 0.79 km is obtained along with a time span of 30 s, another 6-g turn and full throttle is commanded. After approximately 30 s, a 7-g turn is performed; upon completion of the turn, straight and level, nonaccelerating flight is maintained for the completion of the trajectory. The σ_{ave} is 1.9 m^2; RGPO starts after 15, 75, and 102 s; and the SOJ is within 2 degrees of the target LOS from 69 to 76 s and 98 to 126 s.

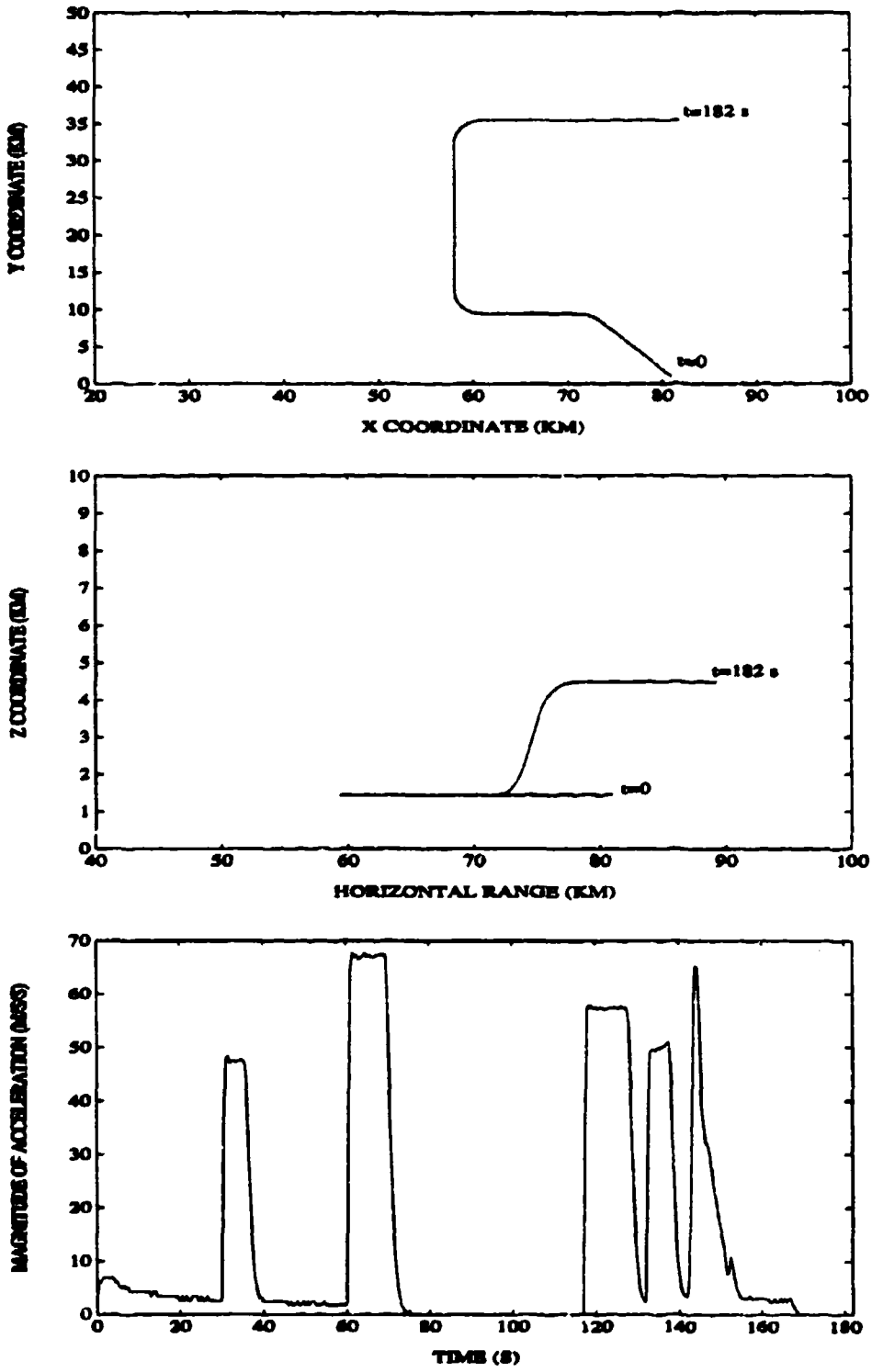

Figure 4.5 Trajectory for Target 5

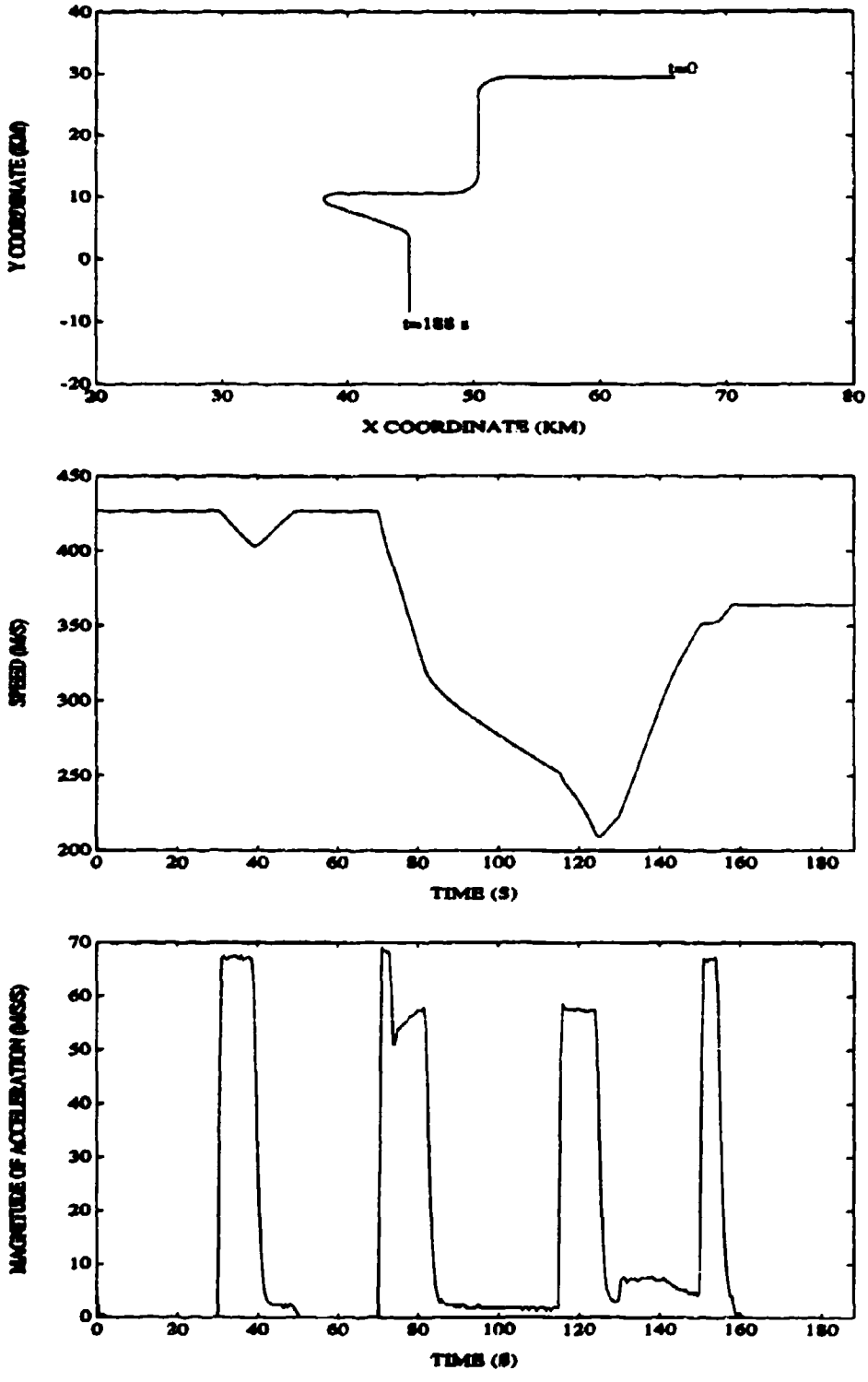

Figure 4.6 Trajectory for Target 6

CHAPTER 5
TRACKING ALGORITHM

Figure 5.1 shows the input and output of the tracking algorithm. At any revisit time, as many as five dwells of any combination of waveforms in Table 2.2 can be requested by the tracking algorithm. The collection of dwells requested at a given time by the tracking algorithm will be referred to as a dwell set. The tracking algorithm routine will receive for each dwell in the requested set the $\Re_k$, r_k^e, r_k^b, and r_k for each range bin in the range gate, with $\Re_k$ above the commanded SNR threshold $\Re_k^{th}$. Each quantity is provided to the tracking algorithm in a matrix where columns 1 through 5 correspond to dwells 1 through 5 of the requested set, respectively. Also, indicators of coherent/noncoherent detections (not used in this benchmark problem) and the waveforms used in the previous radar dwells are given to the tracking algorithm. Since the first detection occurs on a search dwell, the tracking algorithm will be required to initialize the track from a measurement of range, and the bearing and elevation angles of the beam during the detection (*i.e.*, no monopulse error correction in the first measurement). The time for the next measurement and the pointing commands in range $\hat{r}_k$, bearing $\hat{b}_k$, and elevation $\hat{e}_k$ are computed by the tracking algorithm. The tracking (and radar management) algorithm also requests the type of dwell (*i.e.*, search, track, or passive) and selects a waveform (*i.e.*, pulse length) for active dwells from Table 2.2.

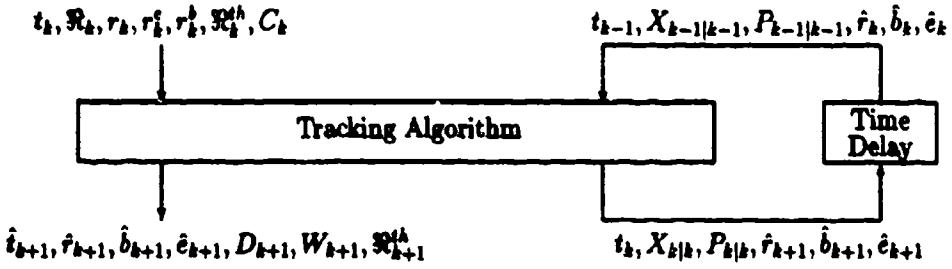

$t_k \triangleq$ Time of previous dwell set

$\Re_k \triangleq$ Observed SNRs on dwells at t_k

$r_k \triangleq$ Range measurements at t_k

$r_k^e, r_k^b \triangleq$ Monopulse ratios in elevation and bearing at t_k

$\Re_k^{th} \triangleq$ SNR detection threshold for dwell set at t_k

$C_k \triangleq$ Indicators of noncoherent detections (*i.e.*, $C_k = 1$)

$\hat{t}_k \triangleq$ Commanded time for next dwell set

$\hat{r}_{k+1}, \hat{b}_{k+1}, \hat{e}_{k+1} \triangleq$ Range, bearing, and elevation for beam pointing control for dwell set at t_{k+1}

$D_{k+1} \triangleq$ Radar dwell type indicator (*i.e.*, search)

$W_{k+1} \triangleq$ Waveform selection at t_{k+1}

$\Re_{k+1}^{th} \triangleq$ SNR detection threshold for dwell set at t_{k+1}

$X_{k|k}, P_{k|k} \triangleq$ Mean and error covariance for target state estimate at time t_k based on measurements through t_k

$$X_k = [\, x_k \quad \dot{x}_k \quad \ddot{x}_k \quad y_k \quad \dot{y}_k \quad \ddot{y}_k \quad z_k \quad \dot{z}_k \quad \ddot{z}_k \,]^T$$

Figure 5.1 Input and Output of the Tracking Algorithm

CHAPTER 6

CRITERIA FOR EVALUATION OF ALGORITHMS

For evaluation of the tracking algorithms, each algorithm shall maintain tracks on the given trajectories with a maximum track loss of 4% and no indication of the target type or number. A track is declared lost if the error in the estimated position of the target is greater than 1 two-way beamwidth in angle or 1.5 range gates (about 2362 m) in range. Since the phased array radar will operate in different environments, the primary measure of tracking performance will be a weighted sum of the average radar energy per second and the average radar time per second. The average energy per second $\overline{E}_{ave}$ is the sum of energy of the track dwells requested by the tracking algorithm divided by the number seconds of the trajectory. The radar energy for a given radar dwell is computed by multiplying the transmit power P_t by the effective pulse width τ_e. The average radar time per second $\overline{T}_{ave}$ is the sum of radar time of the track dwells requested by the tracking algorithm divided by the number of seconds of the trajectory. Each radar dwell requires 0.001 s of radar time. Note that $\overline{T}_{ave}$ is inversely proportional to the average sample period. The quantities $\overline{E}_{ave}$ and $\overline{T}_{ave}$ are computed for each Monte Carlo experiment. Two cost functions for each target are defined as

$$C_1 = \overline{E}_{ave} + 10^3 \overline{T}_{ave} \tag{6.1}$$

$$C_2 = \overline{E}_{ave} + 10^5 \overline{T}_{ave} \tag{6.2}$$

where C_1 corresponds to a period of operation when radar energy is critical, and C_2 corresponds to a period of operation when radar time is critical. Note that the objective is to minimize one of the two cost functions upon request. However, C_1 and C_2 should be computed for each target and presented as the results may indicate the particular benefits of a given algorithm. For a final assessment of algorithm performance, each cost in (6.1) and (6.2) are to be averaged over all the targets, with the costs from Target 1 being counted twice. The algorithm that provides the minimum of both costs by a simple change of the design parameters will be considered the superior algorithm. Note that the energy and radar time during initialization should be included because initialization is a portion of the tracking.

Table 6.1 Summary of Results

Target No.	Time Len (s)	Max Accel (m/s^2)	Man Den (%)	Sample Period (s)	RMSE Pos (m)	RMSE Vel (m/s)	C_1	C_2	Track Lost (%)
1	165	31	29						
2	150	39	34						
3	145	42	36						
4	185	58	46						
5	182	68	70						
6	188	70	59						
Ave*									

* This average is computed with results of Target 1 being counted twice.

A secondary measure of algorithm performance is the computer resources required. Each investigator will present an assessment of the average number of floating point operations per second that their algorithm will require in final implementation. If the algorithm has computational requirements that vary over time, an assessment of the peak number of float point operations per second should also be presented. The average sample periods and Root-Mean-Square Errors (RMSEs) in the position, velocity, and acceleration estimates should be plotted for illustration of algorithm performance. The results should be reported in a table as shown in Table 6.1, where the average of the results are to be reported in the last row. The fourth column indicates the maneuver density which was computed as the percent of the total time that the target acceleration exceeds 5 m/s^2. The fifth column is the average sample period, while the sixth and seventh columns are the RMSE in position and velocity, respectively. The eighth and ninth columns are the costs of (6.1) and (6.2), respectively. The tenth column is the percentage of tracks that are lost during the Monte Carlo simulation.

CHAPTER 7
CONCLUDING REMARKS

When developing a solution to this benchmark problem, one common tracking algorithm should be designed and implemented for all six target trajectories. The tracking algorithm should be designed to address the general specifications of the targets and evaluated with the six trajectories. While the tracking algorithm can adapt to the trajectory, the adaptation should be automatic in that no user-defined inputs denote a target type or specific number. After a table similar to Table 6.1 is completed to summarize the results, the strengths of the solution should be discussed along with the weaknesses. Note that while the best algorithm is the one that minimizes the two cost functions of Section 6, the computational resources required to achieve a given performance are very important when selecting a tracking method for a radar system. Thus, solutions with various computational requirements are of interest. Furthermore, this benchmark problem can be used to illustrate the application of different tracking methods. The computer programs that are enclosed in electronic format allow the effects of the RGPO and/or the SOJ to be easily removed from the simulation program by a simple change of the input file, as discussed in Appendix B.

In the development of this benchmark problem, a number of simplifying assumptions were made in order to limit the scope of the problem and the complexity of the simulation program. First, the targets were modeled as point targets with RCS fluctuations that were independent of the aspect angle of the target with respect to the radar. In an actual radar tracking system, the returns from the targets can occupy multiple range bins, glint errors are common for targets at the closer ranges, and the RCSs of targets can change rapidly when targets maneuver. Second, the effects of closely spaced targets have not been considered. If two targets are separated by less than a beamwidth in angle and their ranges are not fully resolved, the returns from the two targets will interfere. In a monopulse tracking system, this interference can be catastrophic to the tracking. Third, sea-surface induced multipath has been neglected by considering only targets with altitudes above the region where multipath reflections corrupt the monopulse processing. Fourth, the power of the SOJ has been limited

so that it can be defeated with the higher energy waveforms. In an actual system, the SOJ power could require the averaging of the returns from many dwells or coasting the track, while both the target and the SOJ are in the mainbeam. Also, if the SOJ power is sufficiently high, sidelobe jamming can become a serious issue. Fifth, the potential for a jammer onboard the target has been ignored. Sixth, the waveform types have been limited to fixed waveforms with discrete codes. Pulse Doppler and linear Frequency Modulated (FM) waveforms are commonly used radar waveforms, while adapting the discrete coding of the waveforms may prove beneficial in the presence of unresolved targets, multipath, or clutter. Seventh, the effects of background clutter have been neglected. Eighth, track initiation in a cluttered environment has not been considered. Many of this issues are open research problems to be considered in the future.

REFERENCES

1. S. S. Blackman, *Multiple Target Tracking with Radar Applications*, Artech House, Inc., Dedham, MA, 1986.

2. Bar-Shalom and X.R. Li., *Multitarget-Multisensor Tracking: Principles and Techniques*, YBS Publishing, Storrs, CT, 06269-3157, 1995.

3. Y. Bar-Shalom, Ed., *Multitarget-Multisensor Tracking: Advanced Applications, Vol. I*, Artech House, Inc., Dedham, MA, 1991.

4. Y. Bar-Shalom, Ed., *Multitarget-Multisensor Tracking: Applications and Advances, Vol. II*, Artech House, Inc., Dedham, MA, 1992.

5. Y. Bar-Shalom and X.R. Li., *Estimation and Tracking: Principles, Techniques, and Software*, Artech House, Inc., Norwood, MA, 1993.

6. W. D. Blair, G.A. Watson, and S.A. Hoffman, "Benchmark Problem for Beam Pointing Control of Phased Array Radar Against Maneuvering Targets," *Proc. of 1994 American Control Conference*, Baltimore, MD, June 1994, pp. 2071-2075.

7. W. D. Blair, G.A. Watson, G.L. Gentry, and S.A. Hoffman, "Benchmark Problem for Beam Pointing Control of Phased Array Radar Against Maneuvering Targets in the Presence of False Alarms and ECM," *Proc. of 1995 American Control Conference*, Seattle, WA, June 1995, pp. 2601-2605.

8. F. Daum, "A System Approach To Multiple Target Tracking," *Multitarget-Multisensor Tracking: Applications and Advances, Vol. II*, Y. Bar-Shalom, Ed., Artech House, Inc., Dedham, MA, 1992.

9. F. Daum, "Review of 'Multitarget-Multisensor Tracking: Principles and Techniques'," *IEEE Aerospace and Electronic Systems Magazine*, July 1996, pp. 39-42.

10. G. van Keuk and S.S. Blackman, "On Phased-Array Radar Tracking and Parameter Control," *Trans. Aero. Elect. Sys.*, January 1993, pp. 186-194.

11. E. Daeipour, Y. Bar-Shalom, and X. Li, "Adaptive Beam Pointing Control of a Phased Array Radar Using an IMM Estimator," *Proc. of 1994 American Control Conference*, Baltimore, MD, June 1994, pp. 2093-2097.

12. P. Kalata, "An $\alpha - \beta$ Target Tracking Approach to the Benchmark Tracking Problem," *Proc. of 1994 American Control Conference*, Baltimore, MD, June 1994, pp. 2076-2080.

13. C. R. Sastry, B.J. Slocumb, P.D. West, E.W. Kamen, and H.L. Stalford, "Tracking a Maneuvering Target Using Jump Filters," *Proc. of 1994 American Control Conference*, Baltimore, MD, June 1994, pp. 2081-2087.

14. W. D. Blair and G.A. Watson, "IMM Algorithm for Solution to Benchmark Problem for Tracking Maneuvering Targets," *in Acquisition, Tracking, and Pointing VIII*, M.K. Masten, L.A. Stockum, M.M. Birnbaum, G.E. Sevaston, Eds., Proc. SPIE 2221, pp. 303-316, (1994).

15. H. Tsaknakis, and M. Athans, "Tracking Maneuvering Targets Using H_∞ Filters," *Proc. of 1994 American Control Conference*, Baltimore, MD, June 1994, pp. 1796-1805.

16. T. Kirubarajan, Y. Bar-Shalom, W.D. Blair, and G.A. Watson, "IMMPDAF Solution To Benchmark for Radar Resource Allocation and Tracking Targets in the Presence of ECM," submitted for review to *IEEE Trans. Aero. Elect. Sys.*, August 1996.

17. P. D. West, B.J. Slocumb, and E.W. Kamen, "Adaptive Kalman Filter Solution to the Second Benchmark Problem," Final Report for Contract No. N00178-95-M-8217, Naval Surface Warfare Center Dahlgren Division, Dahlgren, VA, January 1996.

18. C. E. Cook and M. Bernfeld, *Radar Signal: An Introduction to Theory and Applications*, Artech House, Inc., Norwood, MA, 1993.

19. B. Edde, *Radar: Principles, Technology, Applications*, Prentice Hall, Englewood Cliffs, NJ, 1993.

20. M. E. Skolnik, *Introduction to Radar Systems, 2nd Ed.*, McGraw-Hill, Inc., New York, NY, 1980

21. S. M. Sherman, *Monopulse Principles and Techniques*, Artech House, Inc., Dedham, MA, 1984.

APPENDIX A

DERIVATION OF MONOPULSE PROCESSING EQUATIONS

While the problem of tracking multiple targets has been studied extensively in recent years, the issue of finite sensor resolution has been completely ignored in almost all of the studies [A-1]. Typically, the targets are assumed to be detected with a given probability of detection in the presence of false alarms and clutter, and the target measurements are modeled as the true values plus independent Gaussian errors [A-2,A-3]. However, when the angular position of a target in the presence of a jammer is measured using a monopulse radar, the Direction-Of-Arrival (DOA) information for the target and jammer are merged into one measurement. DOA estimation for a target in the presence of a Gaussian noise Standoff Jammer (SOJ) is considered in this Appendix. First, some background on monopulse systems and related processing is given along with definitions of the associated notation. Second, the conditional probability density function (pdf) and related statistical properties of monopulse measurements of a target in the presence of a Gaussian SOJ are considered. Third, DOA estimation for an SOJ in the absence of a target is developed. Fourth, the DOA estimation is developed for a target in the absence of an SOJ. Fifth, DOA estimation for a target in the presence of a SOJ is developed utilizing the estimates of Jammer-to-Noise Ratio (JNR) and DOA for the SOJ that can be formed with the measurements in the range gate that do not include the target.

Background and Definitions

In a typical monopulse radar system, the outputs of the receivers are matched filtered, and the in-phase and quadrature portions of the sum and difference signals for the merged measurements of a target and SOJ can be expressed as

$$s_I = \alpha_j \cos\phi_j + \alpha_t \cos\phi_t + n_{SI} \tag{A.1}$$

$$s_Q = \alpha_j \sin\phi_j + \alpha_t \sin\phi_t + n_{SQ} \tag{A.2}$$

$$d_I = \alpha_j\eta_j \cos\phi_j + \alpha_t\eta_t \cos\phi_t + n_{dI} \tag{A.3}$$

$$d_Q = \alpha_j\eta_j \sin\phi_j + \alpha_t\eta_t \sin\phi_t + n_{dQ} \tag{A.4}$$

where

$$\alpha_j = A_j G_\Sigma(\theta_j) \tag{A.5}$$

$$\alpha_t = \sqrt{\kappa} A_t G_\Sigma^2(\theta_t) p_0 \tag{A.6}$$

$$\eta_j = \frac{G_\Delta(\theta_j)}{G_\Sigma(\theta_j)} = \text{ DOA of the SOJ} \tag{A.7}$$

$$\eta_t = \frac{G_\Delta(\theta_t)}{G_\Sigma(\theta_t)} = \text{ DOA of the target} \tag{A.8}$$

$\kappa =$ proportional to the transmitted power

$A_j =$ voltage amplitude of the SOJ

$A_t =$ voltage amplitude of the target backscatter

$G_\Sigma(\theta) =$ sum channel antenna gain at the angle θ

$G_\Delta(\theta) =$ difference channel antenna gain at the angle θ

θ_j = off-boresight angle of the SOJ
θ_t = off-boresight angle of the target
p_0 = matched filter gain
ϕ_j = phase of the SOJ signal
ϕ_t = phase of the target return signal
$n_{SI} \sim N(0, \sigma_S^2)$ $\quad$ $n_{SQ} \sim N(0, \sigma_S^2)$
$n_{dI} \sim N(0, \sigma_d^2)$ $\quad$ $n_{dQ} \sim N(0, \sigma_d^2)$

The n_{SI}, n_{SQ}, n_{dI}, and n_{dQ} are assumed independent. Since the SOJ transmits Gaussian noise, the amplitude of the SOJ A_j will be Rayleigh with parameter A_{j0}, while the amplitude of the target A_t will be assumed fixed since only one observation of the target amplitude is assumed to be available. Then the amplitude of the SOJ signal at the radar is given by

$$f(\alpha_j|\alpha_{j0}) = \frac{\alpha_j}{\alpha_{j0}^2} \exp\left[-\frac{\alpha_j^2}{2\alpha_{j0}^2}\right], \qquad \alpha_{j0} = A_{j0} G_\Sigma(\theta_j) \tag{A.9}$$

Letting Λ and ψ denote the measured amplitude and phase of the sum-signal gives

$$s_I = \Lambda \cos\psi \qquad\qquad s_Q = \Lambda \sin\psi \tag{A.10}$$

where $-\pi < \psi \leq \pi$. The pdf of Λ is found by applying the transformation of random variables in (A.10) to the pdf of s_I and s_Q. Since α_j is Rayleigh distributed and ϕ_j is uniformly distributed on $(-\pi, \pi]$, s_I and s_Q are independent, Gaussian random variables for given values of α_t and ϕ_t. Thus,

$$E[s_I|\Theta] = \alpha_t \cos\phi_t \tag{A.11}$$
$$E[s_Q|\Theta] = \alpha_t \sin\phi_t \tag{A.12}$$

where Θ denotes the parameter set $\{\alpha_{j0}, \eta_j, \alpha_t, \phi_t, \eta_t, \sigma_S, \sigma_d\}$. The variances are given by

$$\mathrm{VAR}[s_I|\Theta] = \mathrm{VAR}[s_Q|\Theta] = \alpha_{j0}^2 + \sigma_S^2 \tag{A.13}$$

Thus, the pdf of Λ is given by

$$f(\Lambda|\Theta) = \frac{\Lambda}{\alpha_{j0}^2 + \sigma_S^2} I_0(\alpha_t \Lambda (\alpha_{j0}^2 + \sigma_S^2)^{-1}) \exp\Big\{-\frac{\Lambda^2 + \alpha_t^2}{2(\alpha_{j0}^2 + \sigma_S^2)}\Big\}, \qquad \Lambda \geq 0 \tag{A.14}$$

where $I_0(\cdot)$ is the zero-order modified Bessel function of the first kind.

In order to write the results of later sections in terms of SNR and JNR, let

$$J = \frac{\alpha_{j0}^2}{\sigma_S^2} \qquad \Re = \frac{\alpha_t^2}{2\sigma_S^2} \qquad \Re_o = \frac{\Lambda^2}{2\sigma_S^2} \tag{A.15}$$

where J represents the JNR of the SOJ, $\Re$ represents the SNR of the target, and $\Re_o$ represents the observed SNR.

The DOA measurements of a monopulse radar are typically taken as the in-phase monopulse ratio [A–4]. With $s = s_I + js_Q$ and $d = d_I + jd_Q$, the in-phase and quadrature monopulse ratios (*i.e.*, measurements) are given by

$$y_I = \mathrm{Re}(\frac{d}{s}) = \frac{d_I s_I + s_Q d_Q}{s_I^2 + s_Q^2} \tag{A.16}$$

$$y_Q = \mathrm{Im}(\frac{d}{s}) = \frac{d_Q s_I - d_I s_Q}{s_I^2 + s_Q^2} \tag{A.17}$$

Distribution of Monopulse Ratio

Since α_j is Rayleigh distributed and ϕ_j is uniformly distributed on $(-\pi, \pi]$, the sum and difference signals are Gaussian distributed given α_t and ϕ_t. The pdf of the sum and difference signals is defined by the mean $\overline{X} = E[X|\Theta]$ and covariance $P = E[(X - \overline{X})(X - \overline{X})^T|\Theta]$, where $X = \begin{bmatrix} s_I & d_I & s_Q & d_Q \end{bmatrix}^T$. Then

$$\overline{X} = \begin{bmatrix} \alpha_t \cos\phi_t \\ \alpha_t \sin\phi_t \\ \alpha_t\eta_t \cos\phi_t \\ \alpha_t\eta_t \sin\phi_t \end{bmatrix} \qquad P = \begin{bmatrix} p_{11} & p_{12} & 0 & 0 \\ p_{12} & p_{22} & 0 & 0 \\ 0 & 0 & p_{11} & p_{12} \\ 0 & 0 & p_{12} & p_{22} \end{bmatrix} \tag{A.18}$$

where

$$p_{11} = \alpha_{j0}^2 + \sigma_S^2 \tag{A.19}$$

$$p_{12} = \alpha_{j0}^2\eta_j \tag{A.20}$$

$$p_{22} = \alpha_{j0}^2\eta_j^2 + \sigma_d^2 \tag{A.21}$$

The inverse and determinant of P are given by

$$P^{-1} = \frac{1}{(p_{11}p_{22} - p_{12}^2)} \begin{bmatrix} p_{22} & -p_{12} & 0 & 0 \\ -p_{12} & p_{11} & 0 & 0 \\ 0 & 0 & p_{22} & -p_{12} \\ 0 & 0 & -p_{12} & p_{11} \end{bmatrix} \tag{A.22}$$

$$|P| = (p_{11}p_{22} - p_{12}^2)^2 \tag{A.23}$$

Then

$$f(X|\Theta) = \frac{1}{4\pi^2(p_{11}p_{22} - p_{12}^2)} \times \exp\left\{ -\frac{p_{11}}{2(p_{11}p_{22} - p_{12}^2)} \left[\frac{p_{22}}{p_{11}} \left((s_I - \alpha_t \cos\phi_t)^2 + (s_Q - \alpha_t \sin\phi_t)^2 \right) \right. \right.$$

$$+\Big((d_I-\alpha_t\eta_t\cos\phi_t)^2+(d_Q-\alpha_t\eta_t\sin\phi_t)^2\Big)$$
$$-\frac{2p_{12}}{p_{11}}\Big((s_I-\alpha_t\cos\phi_t)(d_I-\alpha_t\eta_t\cos\phi_t)$$
$$+(s_Q-\alpha_t\sin\phi_t)(d_Q-\alpha_t\eta_t\sin\phi_t)\Big)\Big]\Big\} \qquad (A.24)$$

Applying the transformation of random variables in (A.10) and

$$d_I=s_Iy_I-s_Qy_Q=y_I\Lambda\cos\psi-y_Q\Lambda\sin\psi \qquad (A.25)$$
$$d_Q=s_Iy_Q+s_Qy_I=y_Q\Lambda\cos\psi+y_I\Lambda\sin\psi \qquad (A.26)$$

gives

$$f(\Lambda,\psi,y_I,y_Q|\Theta)=\frac{\Lambda^3}{4\pi^2(p_{11}p_{22}-p_{12}^2)}\exp\Big\{-\frac{p_{11}}{2(p_{11}p_{22}-p_{12}^2)}\Big[\frac{p_{22}}{p_{11}}\Big(\Lambda^2+\alpha_t^2-2\alpha_t\Lambda\cos\varepsilon\Big)$$
$$-2\frac{p_{12}}{p_{11}}\Big(\Lambda^2y_I-\alpha_t\Lambda y_I\cos\varepsilon+\alpha_t\Lambda y_Q\sin\varepsilon-\alpha_t\Lambda\eta_t\cos\varepsilon+\alpha_t^2\eta_t\Big)$$
$$+\Big(\Lambda^2(y_I^2+y_Q^2)-2y_I\eta_t\alpha_t\Lambda\cos\varepsilon+2y_Q\eta_t\alpha_t\Lambda\sin\varepsilon+\alpha_t^2\eta_t^2\Big)\Big]\Big\} \qquad (A.27)$$

where $\Lambda\geq 0$, $-\infty<y_I<+\infty$, $-\infty<y_Q<+\infty$, and $-\pi-\phi_t<\varepsilon\leq\pi-\phi_t$ with $\varepsilon=\psi-\phi_t$. Then

$$f(\Lambda,\varepsilon,y_I,y_Q|\Theta)=\frac{\Lambda^3}{4\pi^2(p_{11}p_{22}-p_{12}^2)}$$
$$\times\exp\Big\{-\frac{p_{11}}{2(p_{11}p_{22}-p_{12}^2)}\Big[\frac{p_{22}}{p_{11}}\Big(\Lambda^2+\alpha_t^2-2\alpha_t\Lambda\cos\varepsilon\Big)$$
$$+\Lambda^2\Big(y_I^2-2y_I\Big(\frac{p_{12}}{p_{11}}-\Big(\frac{p_{12}}{p_{11}}-\eta_t\Big)\Big)\frac{\alpha_t}{\Lambda}\cos\varepsilon\Big)$$
$$+\Lambda^2\Big(y_Q^2-2y_Q\Big(\frac{p_{12}}{p_{11}}-\eta_t\Big)\frac{\alpha_t}{\Lambda}\sin\varepsilon\Big)$$
$$+2\frac{p_{12}}{p_{11}}\eta_t\alpha_t(\Lambda\cos\varepsilon-\alpha_t)+\alpha_t^2\eta_t^2\Big]\Big\}$$
$$=\frac{\Lambda^3}{4\pi^2(p_{11}p_{22}-p_{12}^2)}$$
$$\times\exp\Big\{-\frac{p_{11}}{2(p_{11}p_{22}-p_{12}^2)}\Big[\Big(\frac{p_{22}}{p_{11}}-\frac{p_{12}^2}{p_{11}^2}\Big)\Big(\Lambda^2+\alpha_t^2-2\alpha_t\Lambda\cos\varepsilon\Big)$$
$$+\Lambda^2\Big(y_I-\Big(\frac{p_{12}}{p_{11}}-\Big(\frac{p_{12}}{p_{11}}-\eta_t\Big)\frac{\alpha_t}{\Lambda}\cos\varepsilon\Big)\Big)^2$$
$$+\Lambda^2\Big(y_Q-\Big(\frac{p_{12}}{p_{11}}-\eta_t\Big)\frac{\alpha_t}{\Lambda}\sin\varepsilon\Big)^2\Big]\Big\} \qquad (A.28)$$

Using (A.14) to condition the pdf of (A.28) on Λ gives

$$f(\varepsilon, y_I, y_Q|\Lambda,\Theta) = \frac{\Lambda^2 p_{11}}{4\pi^2(p_{11}p_{22}-p_{12}^2)I_0(\alpha_t\Lambda p_{11}^{-1})}\exp\left\{\frac{\alpha_t\Lambda}{p_{11}}\cos\varepsilon\right\}$$
$$\times\ \exp\left\{-\frac{p_{11}\Lambda^2}{2(p_{11}p_{22}-p_{12}^2)}\left(y_I-\left(\frac{p_{12}}{p_{11}}-\left(\frac{p_{12}}{p_{11}}-\eta_t\right)\frac{\alpha_t}{\Lambda}\cos\varepsilon\right)\right)^2\right\}$$
$$\times\ \exp\left\{-\frac{p_{11}\Lambda^2}{2(p_{11}p_{22}-p_{12}^2)}\left(y_Q-\left(\frac{p_{12}}{p_{11}}-\eta_t\right)\frac{\alpha_t}{\Lambda}\sin\varepsilon\right)^2\right\} \qquad (A.29)$$

If $\alpha_t = 0$, integrating (A.29) with respect to ε gives

$$f(y_I, y_Q|\Lambda,\Theta,\alpha_t=0) = \frac{\Lambda^2 p_{11}}{2\pi(p_{11}p_{22}-p_{12}^2)}\exp\left\{-\frac{\Lambda^2 p_{11}[y_Q^2+(y_I-p_{12}p_{11}^{-1})^2]}{2(p_{11}p_{22}-p_{12}^2)}\right\}$$
$$= f(y_I|\Lambda,\Theta)f(y_Q|\Lambda,\Theta) \qquad (A.30)$$

where

$$f(y_I|\Lambda,\Theta) = N\left(\frac{p_{12}}{p_{11}}, \frac{p_{11}p_{22}-p_{12}^2}{\Lambda^2 p_{11}}\right) = N\left(\frac{J}{J+1}\eta_j, \frac{1}{2\Re_o}\left[\frac{\sigma_d^2}{\sigma_S^2}+\frac{J}{J+1}\eta_j^2\right]\right) \qquad (A.31)$$

$$f(y_Q|\Lambda,\Theta) = N\left(0, \frac{p_{11}p_{22}-p_{12}^2}{\Lambda^2 p_{11}}\right) = N\left(0, \frac{1}{2\Re_o}\left[\frac{\sigma_d^2}{\sigma_S^2}+\frac{J}{J+1}\eta_j^2\right]\right) \qquad (A.32)$$

and $N(x,y)$ denotes the Gaussian distribution with mean x and variance y. Thus, for the SOJ in the absence of the target, y_I and y_Q are conditionally independent, Gaussian random variables given Λ.

If both targets are on the antenna boresight (*i.e.*, $\eta_j = \eta_t = 0$), (A.29) becomes

$$f(y_I, y_Q|\Lambda,\Theta,\eta_j=\eta_t=0) = f(y_I|\Lambda,\Theta,\eta_j=\eta_t=0)f(y_Q|\Lambda,\Theta,\eta_j=\eta_t=0) \qquad (A.33)$$

where

$$f(y_I|\Lambda,\Theta,\eta_j=\eta_t=0) = N\left(0, \frac{\sigma_d^2}{\Lambda^2}\right) \qquad (A.34)$$

$$f(y_Q|\Lambda,\Theta,\eta_j=\eta_t=0) = N\left(0, \frac{\sigma_d^2}{\Lambda^2}\right) \qquad (A.35)$$

Thus, y_I and y_Q are conditionally independent Gaussian given Λ when $\eta_j = \eta_t = 0$. However, in general (*i.e.*, $\eta_j \neq 0$ or $\eta_t \neq 0$ and $\alpha_t \neq 0$) $f(y_I, y_Q|\Lambda,\Theta)$ has a difficult form for computing the moments directly. Thus, the joint characteristic function [A-5] is used and given by

$$\Phi(\omega_1,\omega_2) = \int_{-\pi}^{\pi}\int_{-\infty}^{\infty}\int_{-\infty}^{\infty}\exp[j\omega_1 y_I + j\omega_2 y_Q]f(\varepsilon, y_I, y_Q|\Lambda,\Theta)\,dy_I\,y_Q\,d\varepsilon$$
$$= \frac{\Lambda^2 p_{11}}{4\pi^2(p_{11}p_{22}-p_{12}^2)I_0(\alpha_t\Lambda p_{11}^{-1})}\int_{-\pi}^{\pi}d\varepsilon\,\exp\left[\frac{\alpha_t\Lambda}{p_{11}}\cos\varepsilon\right]$$

$$\times \int_{-\infty}^{\infty} \exp\left\{ j\omega_1 y_I - \frac{p_{11}\Lambda^2}{2(p_{11}p_{22}-p_{12}^2)}\left(y_I - \left(\frac{p_{12}}{p_{11}} - \left(\frac{p_{12}}{p_{11}} - \eta_t\right)\frac{\alpha_t}{\Lambda}\cos\varepsilon\right)\right)^2 \right\} dy_I$$

$$\times \int_{-\infty}^{\infty} \exp\left\{ j\omega_2 y_Q - \frac{p_{11}\Lambda^2}{2(p_{11}p_{22}-p_{12}^2)}\left(y_Q - \left(\frac{p_{12}}{p_{11}} - \eta_t\right)\frac{\alpha_t}{\Lambda}\sin\varepsilon\right)^2 \right\} dy_Q$$

$$= \frac{1}{2\pi I_0(\alpha_t\Lambda p_{11}^{-1})} \exp\left\{ -\frac{(p_{11}p_{22}-p_{12}^2)}{2p_{11}\Lambda^2}(\omega_1^2+\omega_2^2) + j\omega_1\frac{p_{12}}{p_{11}} \right\}$$

$$\times \int_{-\pi}^{\pi} \exp\left\{ \left(\frac{\alpha_t\Lambda}{p_{11}} - j\omega_1\left(\frac{p_{12}}{p_{11}} - \eta_t\right)\frac{\alpha_t}{\Lambda}\right)\cos\varepsilon + j\omega_2\left(\frac{p_{12}}{p_{11}} - \eta_t\right)\frac{\alpha_t}{\Lambda}\sin\varepsilon \right\} d\varepsilon$$

$$= \frac{1}{I_0(\alpha_t\Lambda p_{11}^{-1})} \exp\left\{ -\frac{(p_{11}p_{22}-p_{12}^2)}{2p_{11}\Lambda^2}(\omega_1^2+\omega_2^2) + j\frac{p_{12}}{p_{11}}\omega_1 \right\}$$

$$\times I_0\left(\frac{\alpha_t}{\Lambda}\sqrt{\left(\Lambda^2 p_{11}^{-1} - j\omega_1(p_{12}p_{11}^{-1}-\eta_t)\right)^2 - \omega_2^2\left(p_{12}p_{11}^{-1}-\eta_t\right)^2}\right) \qquad (A.36)$$

The marginal characteristic functions of y_I and y_Q are then given by

$$\Phi_{y_I}(\omega_1) = \Phi(\omega_1,0) = \frac{1}{I_0(\alpha_t\Lambda p_{11}^{-1})} \exp\left\{ -\frac{(p_{11}p_{22}-p_{12}^2)}{2p_{11}\Lambda^2}\omega_1^2 + j\frac{p_{12}}{p_{11}}\omega_1 \right\}$$

$$\times I_0\left(\frac{\alpha_t}{\Lambda}\left(\Lambda^2 p_{11}^{-1} - j\omega_1(p_{12}p_{11}^{-1}-\eta_t)\right)\right) \qquad (A.37)$$

$$\Phi_{y_Q}(\omega_2) = \Phi(0,\omega_2) = \frac{1}{I_0(\alpha_t\Lambda p_{11}^{-1})} \exp\left\{ -\frac{(p_{11}p_{22}-p_{12}^2)}{2p_{11}\Lambda^2}\omega_2^2 \right\}$$

$$\times\ I_0\left(\frac{\alpha_t}{\Lambda}\sqrt{(\Lambda^4 p_{11}^{-2} - \omega_2^2(p_{12}p_{11}^{-1}-\eta_t)^2}\right) \qquad (A.38)$$

which shows that y_I and y_Q are not Gaussian random variables if $\alpha_t \neq 0$ and $\eta_t \neq p_{12}p_{11}^{-1}$. However, since $\Phi_{y_Q}(\omega_2)$ is real for all ω_2, the pdf of y_Q is symmetrical about zero, which gives $E[y_Q|\Lambda,\Phi] = 0$. Furthermore, since for $\alpha_t \neq 0$ and $\eta_t \neq p_{12}p_{11}^{-1}$,

$$\Phi(\omega_1,\omega_2) \neq \Phi_{y_I}(\omega_1)\Phi_{y_Q}(\omega_2) \qquad (A.39)$$

y_I and y_Q are not in general independent random variables. Setting $s_1 = j\omega_1$ and $s_2 = j\omega_2$ in (A.36) gives the joint moment generating function as

$$M(s_1,s_2) = \frac{1}{I_0(\alpha_t\Lambda p_{11}^{-1})} \exp\left\{ \frac{(p_{11}p_{22}-p_{12}^2)}{2p_{11}\Lambda^2}(s_1^2+s_2^2) + \frac{p_{12}}{p_{11}}s_1 \right\}$$

$$\times I_0\left(\frac{\alpha_t}{\Lambda}\sqrt{(\Lambda^2 p_{11}^{-1} - s_1(p_{12}p_{11}^{-1}-\eta_t))^2 + s_2^2(p_{12}p_{11}^{-1}-\eta_t)^2}\right) \qquad (A.40)$$

The form of (A.40) suggests the use of joint cumulants for the computation of moments of y_I and y_Q. The joint cumulants [A-5] are given by

$$\lambda_{kr} = \frac{\partial^k\partial^r}{\partial s_1^k \partial s_2^r}\Psi(s_1,s_2)\Big|_{s_1=0,s_2=0} \qquad (A.41)$$

where

$$\Psi(s_1,s_2) = = -\ln\left[I_0(\alpha_t \Lambda p_{11}^{-1})\right] + \frac{(p_{11}p_{22}-p_{12}^2)}{2\Lambda^2 p_{11}}(s_1^2+s_2^2) + \frac{p_{12}}{p_{11}}s_1 + \ln\left[I_0\left(\frac{\alpha_t}{\Lambda}\sqrt{\left(\Lambda^2 p_{11}^{-1}-(p_{12}p_{11}^{-1}-\eta_t)s_1\right)^2+(p_{12}p_{11}^{-1}-\eta_t)^2 s_2^2}\right)\right] \quad (A.42)$$

The first-order moments or expected values of y_I and y_Q are given by

$$E[y_I|\Lambda,\Phi] = \lambda_{10} = \frac{\alpha_{j0}^2}{\alpha_{j0}^2+\sigma_S^2}\eta_j - \frac{\alpha_t}{\Lambda}I_{1|0}(\alpha_t\Lambda(\alpha_{j0}^2+\sigma_S^2)^{-1})\left(\frac{\alpha_{j0}^2}{\alpha_{j0}^2+\sigma_S^2}\eta_j-\eta_t\right) \quad (A.43)$$

$$E[y_Q|\Lambda,\Phi] = \lambda_{01} = 0 \quad (A.44)$$

where

$$I_{1|0}(x) = \frac{I_1(x)}{I_0(x)} \quad (A.45)$$

with $I_1(\cdot)$ denoting the first-order modified Bessel function of the first kind. The second central moments of y_I and y_Q are given by

$$\mathrm{VAR}[y_I|\Lambda,\Theta] = \frac{\sigma_S^2}{\Lambda^2}\left[\frac{\sigma_d^2}{\sigma_S^2}+\frac{\alpha_{j0}^2\eta_j^2}{\alpha_{j0}^2+\sigma_S^2}+\frac{\alpha_t^2}{\sigma_S^2}\left(\frac{\alpha_{j0}^2}{\alpha_{j0}^2+\sigma_S^2}\eta_j-\eta_t\right)^2 \times\left[1-I_{1|0}^2(\alpha_t\Lambda(\sigma_{j0}^2+\sigma_S^2)^{-1})-\frac{(\alpha_{j0}^2+\sigma_S^2)}{\alpha_t\Lambda}I_{1|0}(\alpha_t\Lambda(\alpha_{j0}^2+\sigma_S^2)^{-1})\right]\right] \quad (A.46)$$

$$\mathrm{VAR}[y_Q|\Lambda,\Theta] = \frac{\sigma_S^2}{\Lambda^2}\left[\frac{\sigma_d^2}{\sigma_S^2}+\frac{\alpha_{j0}^2\eta_j^2}{\alpha_{j0}^2+\sigma_S^2} + (\alpha_{j0}^2+\sigma_S^2)\frac{\alpha_t}{\sigma_S^2\Lambda}\left(\frac{\alpha_{j0}^2}{\alpha_{j0}^2+\sigma_S^2}\eta_j-\eta_t\right)^2 I_{1|0}(\alpha_t\Lambda(\alpha_{j0}^2+\sigma_S^2)^{-1})\right] \quad (A.47)$$

$$\mathrm{COV}[y_I,y_Q|\Lambda,\Theta] = 0 \quad (A.48)$$

where $\mathrm{VAR}[y_I|\cdot]$ denotes the variance of y_I, and $\mathrm{COV}[y_I,y_Q|\cdot]$ denotes the covariance of y_I and y_Q. While y_I and y_Q are not independent, (A.48) indicates that the random variables are conditionally uncorrelated. Thus, any statistical processing of y_I and y_Q that is based on the first two moments can be accomplished independently. Further analysis that includes the third- and fourth-order marginal cumulants of y_I and y_Q, and the kurtosis as conducted in [A-6] for the case of a single fixed-amplitude target will indicate that y_I and y_Q can be closely approximated as independent, Gaussian random variables.

DOA Estimation for SOJ in the Absence of a Target

Since the energy of the SOJ enters into all of the bins of the range gate, all of the bins can be used to estimate the DOA of the SOJ. Setting $\alpha_t = 0$ in (A.14) and applying the

transformation of (A.15) in (A.14) gives the distribution of the observed Signal-to-Noise Ratio (SNR) of each range bin for measurements of the SOJ as

$$f(\Re_o|J) = \frac{1}{J+1}\exp\Big[-\frac{\Re_o}{J+1}\Big], \qquad \Re_o \geq 0 \tag{A.49}$$

For N samples or range bins, the Maximum Likelihood (ML) estimate of J is given by

$$\hat{J} = Y_N - 1 \tag{A.50}$$

where

$$Y_N = \frac{1}{N}\sum_{i=1}^{N}\Re_{oi} \tag{A.51}$$

with $\Re_{oi}$ denoting the observed SNR for bin i. The estimate $\hat{J}$ is unbiased with variance given by

$$\mathrm{VAR}[\hat{J}|J] = \frac{(J+1)^2}{N} \tag{A.52}$$

Since y_{Ii} and y_{Qi} are Gaussian distributed, the ML estimate of $\bar{y}_I$, the mean of y_I, is given for N range bins by

$$\hat{y}_I = \Big[\sum_{i=1}^{N}\Re_{oi}\Big]^{-1}\sum_{i=1}^{N}\Re_{oi}y_{Ii} \tag{A.53}$$

where $\Re_{oi}$ and y_{Ii} denote the observed SNR and in-phase monopulse ratio for bin i. Thus, the estimate $\hat{y}_I$ is a "power" weighted sum of the N monopulse ratios. Since each y_{Ii} is a Gaussian random variable, $\hat{y}_I$ is the minimum variance estimate of $\bar{y}_I$ and a Gaussian random variable, with variance given by

$$\sigma^2_{\hat{y}_I} = \Big[\sum_{i=1}^{N}2\Re_{oi}\Big]^{-1}p \tag{A.54}$$

where

$$p = \Big[\frac{\sigma_d^2}{\sigma_S^2} + \frac{J}{J+1}\eta_j^2\Big] \tag{A.55}$$

Using the Method of Moments [A-7] estimation and $\hat{y}_I$ to estimate η_j gives

$$\hat{\eta}_j = \Big[1 + \frac{1}{\hat{J}}\Big]\hat{y}_I, \qquad \hat{J} > 3 \text{ dB} \tag{A.56}$$

where JNR has been replaced by its ML estimate since the JNR is typically unknown. Note that $J = \hat{J}$ is a appropriate for $N > 8$.

Using the mean of y_I in (A.31) to form an estimate of p gives an estimate of the variance $\sigma^2_{\hat{y}_I}$ as

$$\hat{\sigma}^2_{\hat{y}_I} = \hat{\sigma}^2_{\hat{y}_Q} = \Big[\sum_{i=1}^{N}2\Re_{oi}\Big]^{-1}\hat{p} \tag{A.57}$$

where

$$\hat{p} = \left[\frac{\sigma_d^2}{\sigma_S^2} + \left(1 + \frac{1}{\hat{J}}\right)\hat{y}_I^2\right], \qquad \hat{J} \geq 3 \text{ dB} \tag{A.58}$$

Using the resulting $\hat{p}$, an estimate of σ_{0i}^2, the variance the monopulse ratios of bin i, can be computed using the N bins according

$$\hat{\sigma}_{0i}^2 = \frac{\hat{p}}{2\Re_{oi}} \tag{A.59}$$

Using (A.56) and (A.57) gives an estimate of the variance associated with $\hat{\eta}_j$ as

$$\hat{\sigma}_{\hat{\eta}_j}^2 = \left[1 + \frac{1}{\hat{J}}\right]^2 \hat{\sigma}_{\hat{y}_I}^2 = \left[1 + \frac{1}{\hat{J}}\right]^2 \left[\sum_{i=1}^{N} 2\Re_{oi}\right]^{-1} \left[\frac{\sigma_d^2}{\sigma_S^2} + \left(1 + \frac{1}{\hat{J}}\right)\hat{y}_I^2\right], \qquad \hat{J} \geq 3 \text{ dB} \tag{A.60}$$

DOA Estimation for Target in the Absence of an SOJ

When a single pulse is used to form a monopulse ratio for DOA estimation, the target amplitude can be treated as fixed and the phase is uniformly distributed in the interval $(-\pi, \pi]$. The target amplitude is observed through the measured amplitude of the sum-signal, where the pdf of Λ is found by setting $\alpha_j = 0$ in (A.14). Applying the transformations of (A.15) in the pdf gives

$$f(\Re_o|\Re) = I_0(2\sqrt{\Re_o \Re}) \exp\{-(\Re_o + \Re)\}, \qquad \Re_o \geq 0 \tag{A.61}$$

Then the ML estimate of $\Re$ based on a single pulse satisfies

$$\sqrt{\frac{\hat{\Re}}{\Re_o}} = I_{1|0}\left(2\sqrt{\hat{\Re}\Re_o}\right) \tag{A.62}$$

where $I_{1|0}(x)$ is defined in (A.45).

The conditional pdf of the y_I, y_Q, and ϵ is found by setting $p_{12} = 0$ in (A.29) to obtain

$$f(\epsilon, y_I, y_Q|\Lambda, \Theta) = \frac{\Lambda^2 \exp\left\{\alpha_t \Lambda \sigma_S^{-2} \cos\epsilon\right\}}{4\pi^2 \sigma_d^2 I_0(\alpha_t \Lambda \sigma_S^{-2})} \exp\left\{-\frac{\Lambda^2}{2\sigma_d^2}\left(y_I - \frac{\alpha_t}{\Lambda}\eta_t \cos\epsilon\right)^2\right\}$$
$$\times \exp\left\{-\frac{\Lambda^2}{2\sigma_d^2}\left(y_Q - \frac{\alpha_t}{\Lambda}\eta_t \sin\epsilon\right)^2\right\} \tag{A.63}$$

Since the location of the pdf of y_Q is independent of η_t (*i.e.*, $E[y_Q|\Lambda, \Theta] = 0$), a single observation of y_Q provides essentially no information concerning the value of η_t. Note that while (A.47) shows that the variance of y_Q depends on η_t, single-pulse estimation of the variance is not considered viable. Noting that the ML value of y_Q is zero and using $y_Q = 0$

in (A.63) gives $\epsilon = 0$. Thus, the ML estimate of η_t for a known target amplitude α_t is given by

$$\hat{\eta}_t = \frac{\Lambda}{\alpha_t} y_I = \sqrt{\frac{\Re_o}{\Re}}\, y_I \qquad (A.64)$$

Comparing (A.64) and (A.43) with $\alpha_{j0} = 0$ clearly indicates that (A.64) gives a biased estimate of η_t. While an unbiased estimate of η_t can be computed with (A.43), the estimate will not be ML. Using $\hat{\eta}_t$ and $\alpha_{j0} = 0$ in (A.46) and (A.47) gives an estimate of the variance of y_I and y_Q as

$$\begin{aligned}\hat{\sigma}^2_{y_I} &= \frac{\sigma_d^2}{\Lambda^2} + y_I^2\left[1 - I^2_{1|0}(\alpha_t\Lambda\sigma_S^{-2}) - \frac{\sigma_S^2}{\alpha_t\Lambda} I_{1|0}(\alpha_t\Lambda\sigma_S^{-2})\right] \\ &= \frac{1}{2\Re_o}\left[\frac{\sigma_d^2}{\sigma_S^2} + 2y_I^2\Re_o\left[1 - I^2_{1|0}(2\sqrt{\Re\Re_o}) - \frac{1}{2\sqrt{\Re\Re_o}} I_{1|0}(2\sqrt{\Re\Re_o})\right]\right] \qquad (A.65)\end{aligned}$$

$$\hat{\sigma}^2_{y_Q} = \frac{\sigma_d^2}{\Lambda^2} + y_I^2\frac{\sigma_S^2}{\alpha_t\Lambda} I_{1|0}(\alpha_t\Lambda\sigma_S^{-2}) = \frac{1}{2\Re_o}\left[\frac{\sigma_d^2}{\sigma_S^2} + 2y_I^2\sqrt{\frac{\Re_o}{\Re}} I_{1|0}(2\sqrt{\Re\Re_o})\right] \qquad (A.66)$$

Using (A.65) and (A.66) gives an estimate of the variance of $\hat{\eta}_t$ for a known target amplitude as $\hat{\sigma}^2_{\eta_t} = \Lambda^2\alpha_t^{-2}\hat{\sigma}^2_{y_I} = \Re_o\Re^{-1}\hat{\sigma}^2_{y_I}$, which is required for tracking with a Kalman filter or Interacting Multiple Model (IMM) algorithm [A-2].

When the target amplitude is unknown to the signal processor, a ML estimate of the target amplitude will be used along with the monopulse ratio to estimate the DOA. Since the target amplitude is observed through the sum-signal, the estimation of the target amplitude will be decoupled from the monopulse processing. Given an observed SNR $\Re_o$, (A.62) gives the ML estimate of $\Re$. Note that $\Re_o$ is a biased observation of $\Re$. An approximate ML estimate is given by

$$\sqrt{\frac{\hat{\Re}}{\Re_o}} \approx \left[\frac{\Re_o}{\Re_o + 0.5}\right], \qquad \Re_o \geq 3 \text{ dB} \qquad (A.67)$$

where the maximum percent error is 5 percent at $\Re_o = 3$ dB. The limitation of $\Re_o \geq 3$ dB is not a particular problem since the detection threshold is often greater than 7 dB and a single observation with a smaller amplitude provides essentially no error reduction relative to the beamwidth of the sum pattern. Thus, using $\hat{\Re}$ for $\Re$ in (A.64) gives an approximately ML estimate of η_t for a monopulse measurement of target with unknown amplitude as

$$\hat{\eta}_t = \left[1 + \frac{\sigma_S^2}{\Lambda^2}\right] y_I = \left[1 + \frac{1}{2\Re_o}\right] y_I\,, \qquad \Re_o > 3 \text{ dB} \qquad (A.68)$$

While (A.68) provides a biased estimate of η_t, the bias will be less than that provided by standard monopulse ratio. A nearly unbiased estimate can be computed by using (A.62) and (A.67) in (A.43) with $\alpha_{j0} = 0$, but the estimate will not be ML. Under the ML conditions of (A.62)

$$\frac{\sigma_S^4}{2\Lambda^4} \approx 1 - I^2_{1|0}(\alpha_t\Lambda\sigma_S^{-2}) - \frac{\sigma_S^2}{\alpha_t\Lambda} I_{1|0}(\alpha_t\Lambda\sigma_S^{-2}) \qquad (A.69)$$

Using (A.69) in (A.65) and (A.62) in (A.66) with $\Re = \hat{\Re}$ gives estimates of the variances of y_I and y_Q as

$$\hat{\sigma}^2_{y_I} = \frac{\sigma_d^2}{\Lambda^2} + \frac{y_I^2\sigma_S^4}{2\Lambda^4} = \frac{1}{2\Re_o}\left[\frac{\sigma_d^2}{\sigma_S^2} + \frac{y_I^2}{4\Re_o}\right], \qquad \Re_o > 3 \text{ dB} \tag{A.70}$$

$$\hat{\sigma}^2_{y_Q} = \frac{\sigma_d^2}{\Lambda^2} + \frac{y_I^2\sigma_S^2}{\Lambda^2} = \frac{1}{2\Re_o}\left[\frac{\sigma_d^2}{\sigma_S^2} + 2y_I^2\right], \qquad \Re_o > 3 \text{ dB} \tag{A.71}$$

Note that $\hat{\sigma}^2_{y_I}$ differs significantly from that reported in [A–4], which is restricted to high SNRs. Monte Carlo simulation studies have been conducted for various values of $\Re$ and η_t to assess the validity of (A.70) for estimating the variances of the corresponding monopulse ratios. For each experiment the amplitude was restricted so that $\Re_o > 3$ dB and $\sigma_d^2 = \sigma_S^2$, and y_I and y_Q were normalized by the corresponding standard deviation of (A.70) before computing the sample standard deviation. The simulation results indicated that the variance estimate of y_I is valid for $3 \le \Re \le 12$ dB with $|\eta_t| < 2$ and for $\Re > 15$ dB with $|\eta_t| < 3$. Note that the variance given in [A–4] was found valid for $\Re \ge 12$ dB and $|\eta_t| < 0.25$. The results for y_Q indicated that $\hat{\sigma}^2_{y_Q}$ is valid for $3 \le \Re \le 9$ dB with $|\eta| < 1$ and $\Re \ge 12$ dB with $|\eta| < 3$.

Using (A.68) and (A.70) gives an estimate of the variance of $\hat{\eta}_t$ as

$$\hat{\sigma}^2_{\hat{\eta}_t} = \left[1 + \frac{\sigma_S^2}{\Lambda^2}\right]^2\left[\frac{\sigma_d^2}{\Lambda^2} + \frac{y_I^2\sigma_S^4}{2\Lambda^4}\right] = \frac{1}{2\Re_o}\left[1 + \frac{1}{2\Re_o}\right]^2\left[\frac{\sigma_d^2}{\sigma_S^2} + \frac{y_I^2}{4\Re_o}\right], \quad \Re_o > 3 \text{ dB} \tag{A.72}$$

which is required for tracking a target with an unknown amplitude. Note that this result differs significantly from [A–4] at low to moderate SNRs.

DOA Estimation for Target in the Presence of a SOJ

When estimating the DOA of a target in the presence of a SOJ, the bins within the range gate that do not include the target can be used to estimate the J and η_j with (A.50) and (A.56) as discussed above. The estimates of J and η_j will then be used with (A.29) to estimate the DOA of the target and (A.46) to estimate the associated variance $\hat{\sigma}^2_{\eta_t}$.

Applying the transformations of (A.15) to the pdf of (A.14) gives

$$f(\Re_o|\Re) = I_0(2\sqrt{\Re_o\Re}(J+1)^{-1})\exp\Big\{-\frac{(\Re_o + \Re)}{(J+1)}\Big\}, \qquad \Re_o \ge 0 \tag{A.73}$$

Then the ML estimate of $\Re$, based on a single pulse given that J is known, satisfies

$$\sqrt{\frac{\hat{\Re}}{\Re_o}} = I_{1|0}\Big(2\sqrt{\hat{\Re}\Re_o}(J+1)^{-1}\Big) \tag{A.74}$$

Given an observed SNR $\Re_o$, (A.74) gives the ML estimate of $\Re$ given that J is known. An approximate ML estimate of $\Re$ is given by

$$\sqrt{\frac{\hat{\Re}}{\Re_o}} \approx \left[\frac{\Re_o}{\Re_o + 0.5(J+1)}\right], \qquad \Re_o > 2J+2 \tag{A.75}$$

Also, under the ML conditions of (A.74),

$$\frac{(J+1)^2}{8\Re_o^2} \approx 1 - I_{1|0}^2(2\sqrt{\Re\Re_o}(J+1)^{-1}) - \frac{J+1}{2\sqrt{\Re\Re_o}} I_{1|0}\left(2\sqrt{\Re\Re_o}(J+1)^{-1}\right), \quad \Re_o > 2J+2 \tag{A.76}$$

Considering J and η_j as known in (A.29) gives a pdf for computing the ML estimate of η_t. Since the location of the pdf of y_Q is independent of η_t (*i.e.*, $E[y_Q|\Lambda,\Theta] = 0$), a single observation of y_Q provides essentially no information concerning the value of η_t. Note that while (A.47) shows that the variance of y_Q depends on η_t, single-pulse estimation of the variance is not considered viable. Noting that the ML value of y_Q is zero and using $y_Q = 0$ in (A.29) gives $\varepsilon = 0$. Thus, the ML estimate of η_t in the presence of a SOJ for a known target amplitude α_t is given by

$$\hat{\eta}_{t|j} = \frac{J}{J+1}\eta_j + \frac{\Lambda}{\alpha_t}\left[y_I - \frac{J}{J+1}\eta_j\right] \tag{A.77}$$

When the target amplitude is unknown, using (A.75) in (A.77) gives

$$\hat{\eta}_{t|j} = \frac{J}{J+1}\eta_j + \left[1 + \frac{J+1}{2\Re_o}\right]\left[y_I - \frac{J}{J+1}\eta_j\right], \quad \Re_o > 2J+2 \tag{A.78}$$

Note that only the mean of the monopulse ratio for the SOJ appears in (A.78). Using M range bins that do not include the target return to estimate J and the mean of the monopulse ratio for the SOJ gives

$$\hat{\eta}_{t|j} = \left[1 + \frac{\hat{J}+1}{2\Re_o}\right] y_I - \left[\frac{\hat{J}+1}{2\Re_o}\right] y_I^j, \quad \Re_o > 2\hat{J}+2 \tag{A.79}$$

where

$$\hat{y}_I^j = \frac{\sum_{i=1}^{M} \Re_{oi} y_{Ii}}{\sum_{k=1}^{M} \Re_{ok}} \tag{A.80}$$

$$\hat{J} = -1 + \frac{1}{N}\sum_{i=1}^{M} \Re_{oi} \tag{A.81}$$

with y_{Ii} and $\Re_{oi}$ denoting the monopulse ratio and observed SNR for bin i that does not include the target return, and y_I and $\Re_o$ denoting the monopulse ratio and observed SNR for the range bin that includes the target detection.

If J and η_j are treated as known in (A.78), then the variance of $\hat{\eta}_{t|j}$ can be related to the variance of y_I, which is given by (A.46). Using the approximation of (A.76) in (A.46) and (A.77) in (A.46) and treating J and η_j as known in (A.78) gives an estimate of the variance of $\hat{\eta}_{t|j}$ as

$$\hat{\sigma}^2_{\hat{\eta}_{t|j}} = \frac{1}{2\Re_o}\left[1+\frac{J+1}{2\Re_o}\right]^2\left[\frac{\sigma_d^2}{\sigma_S^2}+\frac{J}{J+1}\eta_j^2+\frac{(J+1)^2}{4\Re_o}\left(y_I-\frac{J}{J+1}\eta_j\right)^2\right], \quad \Re_o > 2\hat{J}+2 \quad (A.82)$$

Using M range bins that do not include the target return to estimate J and η_j gives

$$\hat{\sigma}^2_{\hat{\eta}_{t|j}} = \frac{1}{2\Re_o}\left[1+\frac{\hat{J}+1}{2\Re_o}\right]^2\left[\frac{\sigma_d^2}{\sigma_S^2}+\left(1+\frac{1}{\hat{J}}\right)(\hat{y}_I^j)^2+\frac{(\hat{J}+1)^2}{4\Re_o}\left(y_I-\hat{y}_I^j\right)^2\right], \quad \Re_o > 2\hat{J}+2 \quad (A.83)$$

where y_I^j and $\hat{J}$ are given by (A.80) and (A.81).

Eq. (A.79) provides an estimate of the DOA of a target in the presence of an SOJ and (A.83) provides an estimate of the variance associated with the DOA estimate. However, note that η_j and J have been used as known quantities. Then a sufficiently large number of range bins should be used to estimate J and η_j. A reasonable criteria for M is $M\hat{J} > 18$ dB. For example, an SOJ with $J = 6$ dB would require about 16 range bins.

REFERENCES

A-1. F. Daum, "Review of 'Multitarget-Multisensor Tracking: Principles and Techniques'," *IEEE Aerospace and Electronic Systems Magazine*, July 1996, pp. 39-42.

A-2. Y. Bar-Shalom and X.R. Li, *Multitarget-Multisensor Tracking: Principles and Techniques*, YBS Publishers, Box U-157, Storrs, CT, 06296-3157, 1995.

A-3. S. S. Blackman, *Multiple-Target Tracking with Radar Applications*, Artech House, Inc., Norwood, MA, 1986.

A-4. S. M. Sherman, *Monopulse Principles and Techniques*, Artech House, Inc., Dedham, MA, 1984.

A-5. A. Papoulis, *Probability, Random Variables, and Stochastic Processes, 3rd Ed.*, McGraw-Hill, Inc., New York, NY, 1991.

A-6. W. D. Blair and M. Brandt-Pearce, "Signal Amplitude Conditioned Density Function for Monopulse Measurements for Fixed-Amplitude Targets," *Proc. of 1996 IEEE National Radar Conf.*, Ann Arbor, MI, May 1996, pp. 374-379.

A-7 H. L. Van Trees, *Detection, Estimation, and Modulation Theory*, John Wiley & Sons, Inc., New York, NY, 1968.

APPENDIX B

DOCUMENTATION OF SIMULATION PROGRAM

A simulation testbed for the Benchmark Problem has been developed by G. A. Watson. The simulation is written in MATLAB for version 4.0. A copy of the simulation code has been provided with this report on computer diskette. A brief explanation of each function of the simulation program is given below.

1. **abs_ied.m** calculates average absolute tracking error for an angle-only filter.
2. **avrg_ied.m** calculates average track filter output values.
3. **bemwdth2.m** calculates the bearing and elevation beamwidths for the given radar model.
4. **bufcl.m** clears the buffer when displaying the status report.
5. **clcspace.m** clears the screen and prints blank lines.
6. **comm2a.m** gates passive dwell measurements.
7. **comm2n.m** gates track and search dwell measurements.
8. **coord.m** converts positions, velocities, and accelerations in Cartesian coordinates to the corresponding spherical coordinate values.
9. **correlr.m** constructs a correlated measurement error covariance matrix.
10. **covplot.m** plots the diagonal elements of the error covariance for a Cartesian track filter.
11. **cvaes96.m** is the primary function for testbed simulation.
12. **cvfilt6.m** is the tracking routine.
13. **fcv.m** creates the constant velocity state transition matrix.
14. **findq.m** creates the process noise covariance matrix.
15. **findra.m** creates an uncorrelated measurement error covariance for a range, bearing, and elevation measurement vector.
16. **gateda.m** performs the measurement update for an angle only track filter.
17. **gatedf.m** performs the measurement update for a track filter using track and search dwell measurements.
18. **gcv.m** creates the constant velocity process error matrix.
19. **hevala.m** converts the predicted state estimate from Cartesian to spherical coordinates.

20. **hprcalca.m** calculates the H matrix for an extended Kalman track filter for three coordinates.

21. **initaper.m** calculates the initial state estimate using a least-squares technique for Cartesian coordinates.

22. **initlbe.m** calculates the initial state estimate using a least-squares technique for angle-only tracking.

23. **ldcvaes6.m** is the default load-in file for **cvaes96**.

24. **makevect.m** makes a vector of uniform random numbers.

25. **makvect2.m** makes a vector of normal random numbers.

26. **pointcv.m** determines where to point the radar for the next dwell using a constant velocity model.

27. **radmod4a.m** is the radar model.

28. **randecm.m** determines random intervals of RGPO.

29. **rmseplot.m** plots the Root-Mean-Square-Error (RMSE) of a Cartesian track filter.

30. **rmse_ied.m** calculates the average RMSE.

31. **sigmaper.m** calculates the initial error covariance matrix using a least-squares technique for Cartesian coordinates.

32. **sigmcobe.m** calculates the initial error covariance matrix using a least-squares technique for angle only tracking.

33. **space.m** prints blank lines.

34. **stdvplot.m** plots the standard deviations of the error covariance for position, velocity, and acceleration for Cartesian track filters.

35. **timer.m** displays how long a simulation will last.

36. **timeup.m** is the time update for a track filter.

37. **trakerr2.m** determines whether the estimation error is above some specified threshold.

38. **voltpat2.m** computes the radar voltage pattern.

39. **zconvert.m** converts the radar measurements to Cartesian coordinates.

Six target trajectories have been provided. The targets are **target1**, **target2**, **target3**, **target4**, **target5** and **target6** and are explained in Chapter 4. There is also a StandOff Jammer (SOJ) trajectory called **jammer**. The target trajectories are generated with a 20 Hz data rate and have the form:

$$[x \quad \dot{x} \quad \ddot{x} \quad y \quad \dot{y} \quad \ddot{y} \quad z \quad \dot{z} \quad \ddot{z} \quad t \quad rcs_{ave} \quad I_{ecm}]^T \tag{B.1}$$

where t is the trajectory time, rcs_{ave} is the average radar cross section of the target, and I_{ecm} is an indicator of on-board target ECM employed during flight. The SOJ trajectory does not have rcs_{ave} and I_{ecm}. The state estimates from the target track filter have the form

$$X^t_{k|k} = [x \quad \dot{x} \quad y \quad \dot{y} \quad z \quad \dot{z} \quad t]^T \tag{B.2}$$

and the state estimates from the SOJ track filter have the form

$$X^j_{k|k} = [b \quad \dot{b} \quad e \quad \dot{e} \quad t]^T \tag{B.3}$$

The target and SOJ state estimates may be saved in the form

$$X^{t,a}_{k|k} = [x \quad \dot{x} \quad \ddot{x} \quad y \quad \dot{y} \quad \ddot{y} \quad z \quad \dot{z} \quad \ddot{z} \quad t]^T \tag{B.4}$$

and

$$X^{j,a}_{k|k} = [b \quad \dot{b} \quad \ddot{b} \quad e \quad \dot{e} \quad \ddot{e} \quad t]^T \tag{B.5}$$

which includes acceleration estimates if desired. The function that calculates the averages output values senses the size of the estimate state vector and performs the calculations accordingly.

The function to run the testbed simulation is **cvaes96**. It has a default load-in file that explains each parameter needed for the track filters. Only output arguments are needed to run **cvaes96** when using the load-in file. The filter parameters are set in the load-in file. The tracking algorithm can also be run using the call-line in **cvaes96**. This is accomplished by passing in all the required parameters specified in the load-in file in the proper location in the call-line. For ease of using the call-line, the parameters are passed to **cvaes96** in the same manner as the output line of the default load-in file. The advantage of using the call-line is that a batch job can be run by varying different input parameters.

There are several outputs from **cvaes96**. If the SOJ is not employed, there will be outputs only for the target. When the SOJ is used, outputs for both the target and SOJ will be given. The outputs of **cvaes96** are given below.

1. **xyz_targ** is the target trajectory.

2. **xyz_jam** is the SOJ trajectory.

3. **ave_filt_targ** is the average target filtered state estimates.

4. **ave_filt_jam** is the average SOJ filtered state estimates.

5. **ave_rmse_targ** is the average target RMSE with the first row being position, the second row velocity, and the third row time. If the state vector has acceleration estimates, the third row is acceleration and the fourth row time.

6. **ave_abs_jam** is the average SOJ absolute track error (ATE) with the first row being bearing, the second row bearing rate, the third row elevation, the fourth row elevation rate, and the fifth row time. If accelerations are calculated, the third row is bearing acceleration, the fourth elevation, the fifth row elevation rate, the sixth row elevation acceleration, and the seventh row time.

7. **ave_cov_targ** is the average of the diagonal elements of the target filtered error covariance.

8. **ave_cov_jam** is the average of the diagonal elements of the SOJ filtered error covariance.

9. **ave_A_targ** is the average target sample period with the first row being the sample period and the second row time.

10. **ave_A_jam** is the average SOJ sample period with the first row being the sample period and the second row time.

11. **ct_targ** is the number of occasions each target state was chosen with the first row being the frequency and the second row time.

12. **ct_jam** is the number of occasions each SOJ state was chosen with the first row being the frequency and the second row time.

13. **ave_iter_targ** is the average number of target updates per run for all maintained tracks.

14. **ave_iter_jam** is the average number of SOJ updates per run for all maintained tracks.

15. **wl_targ** is a matrix specifying when and why target tracks were declared lost. If there are lost target tracks, the first row is the Monte Carlo iteration, the second specifies why the track was lost (lack of measurements = 1, tracking error was above = 2), and the third row is the declaration time.

16. **wl_jam** is a matrix specifying when and why SOJ tracks were declared lost. If there are lost SOJ tracks, the first row is the Monte Carlo iteration, the second specifies why the track was lost (lack of measurements = 1, tracking error was above = 2), and the third row is the declaration time.

17. **perc_targ** has two elements with the first being the percentage of target measurements

detected and the second the percentage of target measurements within the tracking gate.

18. **perc_jam** has two elements with the first being the percentage of SOJ measurements detected and the second the percentage of SOJ measurements within the tracking gate.

19. **ave_dw_targ** is the average dwell time, look energy, and power for each target dwell time.

20. **p_crit** is a performance criteria vector with nine elements and has the form: 1) average target sample period, 2) average dwell time per dwell, 3) average energy per dwell, 4) average dwell time per track length, 5) average energy per track length, 6) average dwell time per run, 7) average energy per run, 8) average position error per dwell, and 9) average velocity error per dwell.

The output **perc_targ** and **perc_jam** are outputs specifically designed for this application to provide further performance evaluation of the algorithm. You may wish to add ones pertinent to your track algorithm. When adaptively sampling the trajectory, the output matrices will be very large because the same sequence of measurements will not be chosen each time. As a result, a running total is kept of how many times each trajectory state was sampled. Since the output matrices are large, you may want to reduce their size by binning the outputs over a specified time interval, such as each 0.5 seconds. The output matrices will contain values if that trajectory state was chosen at least one time for a maintained track. If the state was not chosen, there will be no values in the output matrices corresponding to that time. The binning is accomplished by averaging the outputs over each specified time interval as determined by the time values of the output matrix. There may be different numbers of outputs in each interval depending on whether or not that state was chosen during the simulation. You may wish to average all the values in the time interval or do a weighted average based on the frequency each state in the interval was sampled. This will allow for the trend to be seen without having to plot each output time.

If you have any question about the programs or how to run them, please feel free to contact Greg Watson anytime!! Phone: (540) 653-7378, Email: gawatso@nswc.navy.mil.

DISTRIBUTION

	Copies
DOD ACTIVITIES (CONUS)	
ATTN DR RABINDER MADAN	2
JAMES K HALL	1
WILLIAM J MICELI	1
CODE 313	
OFFICE OF NAVAL RESEARCH	
800 N QUINCY ST	
ARLINGTON VA 22217-5660	
ATTN DR JOE LAWRANCE	1
CODE 5740	
NRL	
WASHINGTON DC 20375	
DEFENSE TECHNICAL INFORMATION CENTER	
8725 JOHN J KINGMAN ROAD	
SUITE 0944	
FT BELVOIR VA 22060-6218	2
ATTN CODE E29L	
TECHNICAL LIBRARY	1
COMMANDING OFFICER	
CSSDD NSWC	
6703 W HIGHWAY 98	
PANAMA CITY FL 32407-7001	
NON-DOD ACTIVITIES (CONUS)	
THE CNA CORPORATION	
P O BOX 16268	
ALEXANDRIA VA 22302-0268	2
ATTN GIFT AND EXCHANGE DIVISION	4
LIBRARY OF CONGRESS	
WASHINGTON DC 20540	
ATTN DR YAAKOV BAR-SHALOM	2
ESE DEPT U-157	
260 GLENBROOK RD	
STORRS CT 06269-3157	
ATTN DR MAITE BRANDT-PEARCE	1
DEPT OF ELECTRICAL ENGINEERING	
UNIVERSITY OF VIRGINIA	
CHARLOTTESVILLE VA 22903-2442	
ATTN DR RAMAN K MEHRA	1
DR CONSTANTINO RAGO	1
SCIENTIFIC SYSTEMS	
500 W CUMMINGS PK SUITE 3950	
WOBURN MA 01801	
ATTN PHILIP O WEST	1
BENJAMIN J SLOCUMB	1
GEORGIA TECH RESEARCH INSTITUTE	
ELECTRONIC SYSTEMS LABORATORY	
CONCEPTS ANALYSIS DIVISION	
ATLANTA GA 30332-0800	
ATTN MELVIN BELCHER JR	1
GEORGIA TECH RESEARCH INSTITUTE	
SENSORS AND ELECTROMAGNETIC LABORATORY	
RADAR SYSTEMS DIVISION	
ATLANTA GA 30332-0800	
ATTN DR EDWARD KAMEN	1
SCHOOL OF ELECTRICAL AND COMPUTER ENGINEERING	
GEORGIA INSTITUTE OF TECHNOLOGY	
ATLANTA GA 30332	
ATTN DR PAUL SINGER	2
SAM BLACKMAN	1
ROBERT POPLI	1
DOREEN SASAKI	1
HUGHES AIRCRAFT	
EO E1 MAIL STOP B102	
PO BOX 902	
EL SEGUNDO CA 90245	
ATTN DR OLIVER E DRUMMOND	1
10705 CRANKS RD	
CULVER CITY CA 90250	

DISTRIBUTION (Continued)

	Copies
ATTN JOSEPH S PRIMERANO	1
CHRISTOPHER KNOWLTON	1
PLANNING CONSULTANT INC	
PO BOX 1676	
DAHLGREN VA 22448	
ATTN DR LON CARPENTER	1
DR EDWARD PRICE	1
UNITED DEFENSE	
1 DANUBE DR	
KING GEORGE VA 22485	
ATTN DR KUO CHU CHANG	1
DEPT OF SYSTEMS ENGINEERING	
SCHOOL OF INFORMATION	
TECHNOLOGY AND ENGINEERING	
GEORGE MASON UNIVERSITY	
FAIRFAX VA 22030-4444	
ATTN DR XIA-RONG LI	2
EE DEPT	
UNIVERSITY OF NEW ORLEANS	
NEW ORLEANS LA 70148	
ATTN DR A T ALOUANI	1
J N ANDERSON	1
P K RAJAN	1
DEPT OF ELECTRICAL AND COMPUTER	
ENGINEERING	
TTU BOX 05004	
COOKEVILLE TN 38505	
ATTN DR PAUL KALATA	1
ECE DEPT	
DREXEL UNIVERSITY	
PHILADELPHIA PA 19104	
ATTN GLENN WOODARD	1
GARY L HILD	1
ANDREW MITTURA	1
LOGICON/SYSCON CORPORATION	
PO BOX 1480	
DAHLGREN VA 22448-1480	
ATTN GRANISON S GERRISON	1
NICHOLS RESEARCH CORPORATION	
P O BOX 400002	
HUNTSVILLE AL 35805-1502	

	Copies
ATTN FRANK REIFLER	1
LOCKHEED MARTIN	
GOVERNMENT ELECTRONIC SYSTEMS	
MISSILE SYSTEM DESIGN	
199 BORTON LANDING RD	
MOORESTOWN NJ 08057-3075	
ATTN BOB OTTINGER	1
INGAR BLOSFELDS	1
LOCKHEED MARTIN GES	
NAVAL ADVANCED SYSTEMS	
BUILDING 127-207	
BORTON LANDING RD	
MOORESTOWN NJ 08057	
ATTN DR DAVID CASTANON	1
DEPT OF ELECTRICAL COMPUTER AND	
SYSTEMS ENGINEERING	
BOSTON UNIVERSITY	
44 CUMMINGTON ST	
BOSTON MA 02215	
ATTN WILLIAM M STONESTREET	1
ALAN WILLSKY	1
ALPHATECH INC	
EXECUTIVE PLACE III	
50 MALL RD	
BURLINGTON MA 01803	
ATTN MICHAEL ATHANS	1
ROOM 35-406	
DEPT OF EE	
MIT	
CAMBRIDGE MA 02139	
NON-DOD ACTIVITIES (EX-CONUS)	
ATTN DR NEIL GORDON	1
WEAPONS SYSTEMS SECTOR	
DRA FAMBOROUGH	
HAMPSHIRE	
GU14 6TD UK	
ATTN DR ALFONSO FARINA	2
SYSTEMS ANALYSIS GROUP ALENIA	
VIA TIBURTINA KM 12.400,00131	
ROME ITALY	

DISTRIBUTION (Continued)

		Copies
INTERNAL		
A20	BEUGLASS	1
A50	LUCAS	1
B05	STATON	1
B30		1
B32		1
B32	BLAIR	30
B32	CONTE	1
B32	GENTRY	1
B32	GROVES	1
B32	HELMICK	1
B32	RICE	1
B32	WERME	1
B32	WATSON	4
B35	BAILEY	1
B35	FENNEMORE	1
B35	HARRISON	1
E231		3
E282	WAITS	1
F10	KNICELY	1
F20		1
F40		1
F40	STAPLETON	1
F406		1
F41	FONTANA	1
F41	MARTIN	1
F41	PAWLAK	1
F42	CALDWELL	1
F42	KLOCKAK	1
F42	LEONG	1
G23	GRAFF	1
N24	BOYER	1
N24	MURRAY	1
N92	LABERTSON	1
N92	FOSTER	1
N92	GRAY	1